ANNUAL REVIEWS **Further**

**Click here** for quick links to Annual Reviews content online, including:

- Other articles in this volume
- Top cited articles
- Top downloaded articles
- Our comprehensive search

Annu. Rev. Fluid Mech. 2011.43:219-245. Downloaded from www.annualreviews.org
by JOHNS HOPKINS UNIVERSITY on 03/17/11. For personal use only.

# Lagrangian Dynamics and Models of the Velocity Gradient Tensor in Turbulent Flows

Charles Meneveau

Department of Mechanical Engineering and Center of Environmental and Applied Fluid Mechanics, Johns Hopkins University, Baltimore, Maryland 21218; email: meneveau@jhu.edu

Annu. Rev. Fluid Mech. 2011. 43:219–45

First published online as a Review in Advance on August 24, 2010

The *Annual Review of Fluid Mechanics* is online at fluid.annualreviews.org

This article's doi: 10.1146/annurev-fluid-122109-160708

Copyright © 2011 by Annual Reviews. All rights reserved

0066-4189/11/0115-0219$20.00

## Keywords

turbulence, vorticity, stochastic differential equation, statistical geometry, intermittency

## Abstract

Many fundamental and intrinsic properties of small-scale motions in turbulence can be described using the velocity gradient tensor. This tensor encodes interesting geometric and statistical information such as the alignment of vorticity with respect to the strain-rate eigenvectors, rate of deformation and shapes of fluid material volumes, non-Gaussian statistics, and intermittency. In the inertial range of turbulence, similar properties can be described using the coarse-grained or filtered velocity gradient tensor. In this article we review various models that aim at understanding these phenomena using a small number of ordinary differential equations, written either as a low-dimensional dynamical system or as a set of stochastic differential equations. Typically these describe the Lagrangian evolution of the velocity gradient tensor elements following fluid particles and require models for the pressure Hessian and viscous effects. Sample results from various models are shown, and open challenges are highlighted.

Annu. Rev. Fluid Mech. 2011.43:219-245. Downloaded from www.annualreviews.org
by JOHNS HOPKINS UNIVERSITY on 03/17/11. For personal use only.

## 1. INTRODUCTION AND PHENOMENA

Gradient fields of fluid velocity provide a rich characterization of the local quantitative and qualitative behavior of flows. This observation is evident from the linear approximation of the velocity field $\mathbf{u}(\mathbf{x}, t)$ surrounding an arbitrary point in the flow, $\mathbf{x}_0$:

$$u_i(\mathbf{x}, t) = u_i(\mathbf{x}_0, t) + A_{ij}(\mathbf{x}_0, t)(x_j - x_{0j}) + \cdots, \tag{1}$$

where the velocity gradient tensor $\mathbf{A}$ has been defined according to

$$A_{ij} = \frac{\partial u_i}{\partial x_j}. \tag{2}$$

If moving locally with the fluid velocity $\mathbf{u}(\mathbf{x}_0, t)$, $\mathbf{A}$ determines the local velocity field surrounding the observer. The linear expansion is limited to a neighborhood over which $\mathbf{u}$ is sufficiently smooth and the variations in velocity gradient are small. In turbulent flows, such neighborhoods are on the order of the Kolmogorov scale $\eta_K = (\nu^3/\langle\epsilon\rangle)^{1/4}$, where $\nu$ is the fluid kinematic viscosity and $\langle\epsilon\rangle$ is the mean rate of dissipation of kinetic energy.

The second-rank tensor $\mathbf{A}$ encodes rich information about the flow through its nine components (in three dimensions). A natural decomposition separates $\mathbf{A}$ into its symmetric part (the strain-rate tensor $\mathbf{S}$) and its antisymmetric part (the rotation-rate tensor $\mathbf{\Omega}$) according to

$$A_{ij} = S_{ij} + \Omega_{ij}, \quad \text{where} \quad S_{ij} = \frac{1}{2}(A_{ij} + A_{ji}), \quad \Omega_{ij} = \frac{1}{2}(A_{ij} - A_{ji}). \tag{3}$$

We are mostly concerned with incompressible flows for which the velocity field is divergence free, and thus $A_{kk} = S_{kk} = \lambda_\alpha + \lambda_\beta + \lambda_\gamma = 0$, where the $\lambda$'s are the three (real) eigenvalues of $\mathbf{S}$. In the nondegenerate case of unequal eigenvalues, $\mathbf{S}$ has three orthogonal eigenvectors that define the principal axes of $\mathbf{S}$. These indicate the directions of the maximum rate of fluid extension ($\lambda_\alpha > 0$) and contraction ($\lambda_\gamma < 0$) and an intermediate fluid deformation that can be either extending or contracting in the third direction. The rotation tensor, $\mathbf{\Omega}$, describes the magnitude and direction of the rate of rotation of fluid elements. It is related to the vorticity vector $\boldsymbol{\omega} = \nabla \times \mathbf{u}$ according to $\omega_i = -\varepsilon_{ijk}\Omega_{jk}$, where $\varepsilon_{ijk}$ is the alternating tensor (and $\Omega_{ij} = -\frac{1}{2}\varepsilon_{ijk}\omega_k$).

As a traceless, second-rank tensor in three dimensions, $\mathbf{A}$ contains eight independent elements, and it can be characterized by $8 - 3 = 5$ intrinsic, orientation-invariant scalars (three scalars are required to specify the orientation of a frame in three dimensions). The five scalars can be the two independent eigenvalues of $\mathbf{S}$ and the three vorticity components in the $\mathbf{S}$ eigensystem, or appropriately defined tensor contractions. It is convenient to define the following five scalar invariants (Cantwell 1992, Martin et al. 1998b):

$$Q = -\frac{1}{2}A_{im}A_{mi}, \quad R = -\frac{1}{3}A_{im}A_{mn}A_{ni}, \tag{4}$$

$$Q_S = -\frac{1}{2}S_{im}S_{mi}, \quad R_S = -\frac{1}{3}S_{im}S_{mn}S_{ni}, \quad V^2 = S_{in}S_{im}\omega_m\omega_n. \tag{5}$$

Over the past two decades, the rapidly expanding power of direct numerical simulations (DNS) (Ishihara et al. 2009) and recent developments in experimental techniques (Wallace 2009, Katz & Sheng 2010, Wallace & Vukoslavcevic 2010) have provided access to the full velocity gradient tensor in a variety of turbulent flows. As a result, rather surprising phenomena have been observed, as summarized below.

### 1.1. Phenomena

**Preferential vorticity alignment.** Using DNS of isotropic turbulence, Ashurst et al. (1987) found that when sampling arbitrary points in a turbulent flow, the most likely alignment of the

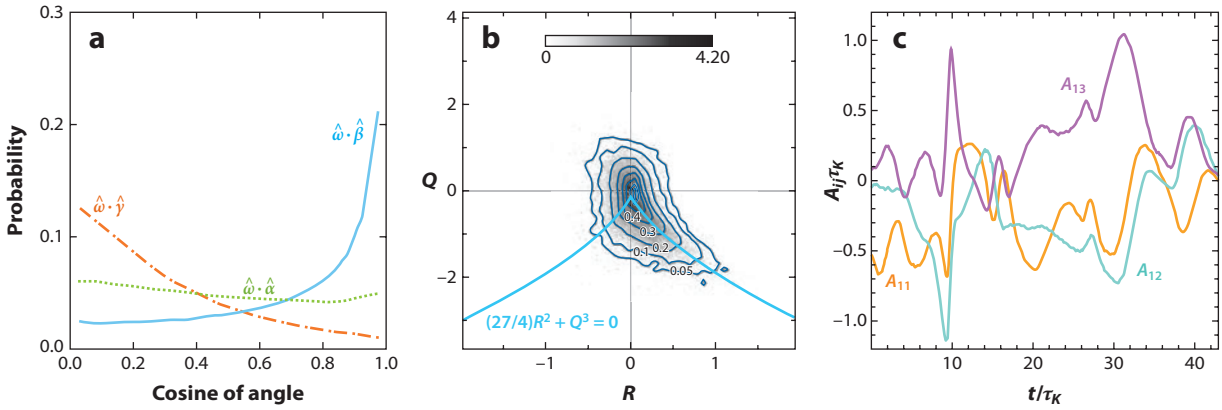


**Figure 1**

Sample results from direct numerical simulation and experiments illustrating interesting geometric and statistical phenomena characterizing the velocity gradient tensor in turbulence. (*a*) Probability density function (PDF) of the cosine of the angle between vorticity and eigenvectors of the strain-rate tensor. Figure adapted from Ashurst et al. (1987). (*b*) Joint PDF of $R$ and $Q$, measured in a high–Reynolds number atmospheric boundary layer using hot-wire anemometry. Figure reproduced from Gulitski et al. (2007). (*c*) Sample time histories of individual elements $A_{ij}(t)$ computed by following fluid particles across a Web-based database of isotropic turbulence (Li et al. 2008).

vorticity vector $\boldsymbol{\omega}$ with respect to the principal axes of $\mathbf{S}$ was with the intermediate eigenvector $\boldsymbol{\beta}_S$, the direction corresponding to the eigenvalue $\lambda_\beta$ that could be either positive or negative. That is to say, measured probability density functions (PDFs) of the cosine of the angle between both vectors, $\cos\theta_{\omega\beta} = \frac{\boldsymbol{\omega}}{|\omega|}\cdot\boldsymbol{\beta}_S$, showed a strong peak at $\cos\theta_{\omega\beta} = 1$, i.e., a most likely behavior of strong alignment with $\theta_{\omega\beta} = 0$ (see **Figure 1*a***). This trend has been confirmed in various flows also based on multiprobe hot-wire experimental data, e.g., by Tsinober et al. (1992) and Gulitski et al. (2007), and using optical techniques by Lüthi et al. (2005) and Mullin & Dahm (2006). For a random structureless gradient field, the PDF of $\cos\theta_{\omega\beta}$ is uniform between $-1$ and $+1$.

**Local structure of fluid deformation rate.** In examining PDFs of the individual eigenvalues of $\mathbf{S}$, Kerr (1987) and Ashurst et al. (1987) observed that the most likely value of $\lambda_\beta$ was positive. This was confirmed using hot-wire experimental data (Tsinober et al. 1992, Gulitski et al. 2007). Noting that the three eigenvalues are statistically dependent on one another (e.g., their sum vanishes), Lund & Rogers (1994) defined a dimensionless parameter that depends on the three eigenvalues according to

$$s^* = -\frac{3\sqrt{6}\,\lambda_\alpha\lambda_\beta\lambda_\gamma}{(\lambda_\alpha^2+\lambda_\beta^2+\lambda_\gamma^2)^{3/2}}. \qquad (6)$$

This parameter is bounded between $s^* = -1$ and $s^* = 1$, and for a Gaussian random velocity gradient field with no preferred structure, the PDF of $s^*$ is uniform. Lund & Rogers (1994) observed from DNS that the PDF of $s^*$ is peaked strongly at $s^* = 1$, which is equivalent to $\lambda_\alpha = \lambda_\beta = -\frac{1}{2}\lambda_\gamma > 0$. That is to say, the most likely state of the straining in turbulence is axisymmetric extension in which a small spherical fluid element moving with the flow extends in two directions and contracts in the third, forming a disk-like structure.

**Skewed joint probability density function of *R*-*Q* invariants.** Measurements of the invariants $R$ and $Q$ show that their joint PDF has a very particular shape, similar to an inverted and sheared



Annu. Rev. Fluid Mech. 2011.43:219-245. Downloaded from www.annualreviews.org
by JOHNS HOPKINS UNIVERSITY on 03/17/11. For personal use only.

drop (Cantwell 1993). There is a marked increased probability of points where $R > 0$ and $Q < 0$, mostly along the so-called Vieillefosse tail $Q = -\frac{3}{2^{2/3}} R^{2/3}$. Such a trend occurs in a variety of flows as confirmed in DNS (e.g., Chong et al. 1998, Nomura & Post 1998, Soria et al. 1998, Ooi et al. 1999, Lüthi et al. 2009) and experiments (Gulitski et al. 2007, Tsinober 2009, Elsinga & Marusic 2010). **Figure 1*b*** shows a sample joint PDF obtained from experimental data (Gulitski et al. 2007).

**Skewness and intermittency.** As reviewed by Sreenivasan & Antonia (1997), the longitudinal velocity gradient is negatively skewed, e.g., in some arbitrary direction $x_1$, $\mathcal{S}_A = \langle A_{11}^3 \rangle / \langle A_{11}^2 \rangle^{3/2} \approx -0.5$, slowly becoming more negative with increasing Reynolds number. The PDFs of longitudinal and transverse gradients, e.g., $A_{11}$ and $A_{12}$, display elongated stretched exponential tails (see, e.g., Castaing et al. 1990, Kailasnath et al. 1992, Frisch 1995, Chevillard et al. 2006). **Figure 1*c*** shows several representative time series of $A_{ij}$ obtained by following fluid particles in a DNS of isotropic turbulence at $R_\lambda = 430$. The signals show some violent excursions far from their mean value. Higher-order moments of $A_{11}$ such as the flatness (kurtosis) coefficient $\mathcal{K}_A = \langle A_{11}^4 \rangle / \langle A_{11}^2 \rangle^2$ grow rapidly with Reynolds number and significantly exceed the values for Gaussian statistics. This behavior indicates that extremely large values of velocity gradients are much more probable than what a Gaussian distribution would predict. In fact, moments of the gradients scale in nontrivial (anomalous) ways with the Reynolds number (Nelkin 1990, Sreenivasan & Antonia 1997). Another well-known feature of small-scale turbulence is that the dissipation rate $\epsilon = 2\nu S_{ij} S_{ij}$ displays large levels of intermittency (see, e.g., Meneveau & Sreenivasan 1991; Zeff et al. 2003; Ishihara et al. 2009, figure 4), nearly log-normal statistics (Frisch 1995), and a variance (of its logarithm) that increases with the Reynolds number in a particular way. Similar trends hold for the pseudodissipation, $\epsilon' = \nu A_{ij} A_{ij}$, and as observed by Yeung & Pope (1989) and Yeung et al. (2005), its statistics appear to conform more closely to log-normality than $\epsilon$.

**Coarse-grained or filtered velocity gradient.** The phenomena described above relate to the velocity gradient field that, in high–Reynolds number turbulent flows, is dominated by the smallest, viscous scales of motion. A substantial amount of research has been devoted to the statistical features of velocity increments in the inertial range (Anselmet et al. 1984, Frisch 1995, Sreenivasan & Antonia 1997). Moments of $\delta_\ell u = [u_i(\mathbf{x} + \boldsymbol{\ell}) - u_i(\mathbf{x})](\ell_i / ||\boldsymbol{\ell}||)$ (the longitudinal velocity increments at scale $\ell$) have received considerable attention, in particular, their scaling exponents $\xi_p$ from $\langle \delta_\ell u^p \rangle \sim \ell^{\xi_p}$ and the shape of their PDFs that display increasingly long tails as $\ell$ decreases. Transverse velocity increments $\delta_\ell v$ can be defined accordingly. A relationship between velocity increments at scale $\ell$ and velocity gradients coarse-grained (or filtered) at scale $\ell$ can be established. Heuristically, the scaling relationship is $\ell \tilde{A}_{11} \sim \delta_\ell u$ and $\ell \tilde{A}_{12} \sim \delta_\ell v$, where $\tilde{\mathbf{A}} = G_\ell * \mathbf{A}$ is the filtered or coarse-grained velocity tensor ($G_\ell$ is a convolution kernel of characteristic scale $\ell$). Thus, it is expected that $\langle \tilde{A}_{11}^p \rangle \sim \ell^{\xi_p - p}$ and that therefore the study of moments and PDFs of velocity increments in the inertial range can also proceed using elements of the coarse-grained velocity gradient tensor. It has been shown that the geometric trends mentioned above are also shared by the coarse-grained velocity gradient tensor, although the quantitative details depend weakly on scale. For instance, Borue & Orszag (1998) and Chertkov et al. (1999) provide joint PDFs of $R$ and $Q$ at various scales obtained from DNS (see **Figures 2*a*,*b*** for results at $2\eta_K$ and $8\eta_K$). Van der Bos et al. (2002) evaluated the joint PDF at $30\eta_K$, and **Figure 2*c*** shows experimental data in pipe flow collected using a holographic optical measurement technique (Tao et al. 2002). Coarse-grained vorticity alignments and the preferential structure of filtered strain-rate eigenvalues in atmospheric turbulence have been studied by Higgins et al. (2003).



Annu. Rev. Fluid Mech. 2011.43:219-245. Downloaded from www.annualreviews.org
by JOHNS HOPKINS UNIVERSITY on 03/17/11. For personal use only.

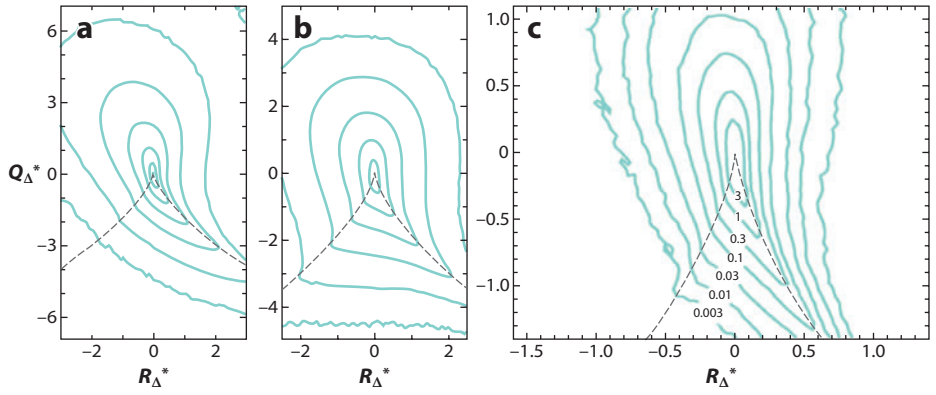


**Figure 2**

Joint probability density function of $R$ and $Q$ measured from filtered direct numerical simulation data at scales (*a*) $\Delta = 2\eta_K$ and (*b*) $8\eta_K$ and (*c*) from holographic particle image velocimetry data at scale $30\eta_K$. Panels *a* and *b* adapted from Chertkov et al. (1999) and panel *c* adapted from Van der Bos et al. (2002).

## 1.2. Dynamical Equation for the Velocity Gradient Tensor

The prior section has reviewed the main phenomena characterizing the single-point statistical properties of the velocity gradient tensor in three-dimensional (3D) turbulence that will be discussed here. The focus of the present article is to review a particular subset of the literature dealing with attempts to understand these phenomena from terms in the Navier-Stokes equations. Furthermore, the works reviewed all have in common that they express the time evolution of $\mathbf{A}$ (or $\tilde{\mathbf{A}}$) following fluid particles (Lagrangian description) as a set of ordinary differential equations (ODEs) or stochastic differential equations. They do not attempt to say anything about the velocity field that advects the fluid particles. Hence, solving field equations is not envisioned. We do not cover the many interesting works that, in a complementary approach to the ones reviewed here, attempt to explain the above phenomena by focusing on properties of coherent flow structures (see, e.g., Jimenez 1992, Brasseur & Lin 2002).

The time evolution of $\mathbf{A}$ following fluid particles can be obtained quite simply by taking the gradient of the Navier-Stokes equations $[\frac{\partial}{\partial x_j}(N.S.)_i]$. For incompressible flow, the resulting equation reads

$$\frac{dA_{ij}}{dt} = -A_{ik}A_{kj} - \frac{\partial^2 p}{\partial x_i \partial x_j} + \nu \frac{\partial^2 A_{ij}}{\partial x_k \partial x_k}, \tag{7}$$

where $d/dt$ stands for the Lagrangian material derivative (i.e., $d/dt \equiv \partial/\partial t + u_k \partial/\partial x_k$), $p$ is the pressure divided by the density of the fluid, and $\nu$ is the kinematic viscosity. Equation 7 is not closed in terms of $\mathbf{A}$ at position $\mathbf{x}$ and time $t$ due to the last two terms in the right-hand side of the equation, the pressure Hessian $\partial^2 p/\partial x_i \partial x_j$ and the viscous term $\nu \nabla^2 A_{ij}$. The trace of the above equation with the incompressibility condition $A_{ii} = 0$ leads to the Poisson equation $\nabla^2 p = -A_{lk}A_{kl}$, showing that the pressure field is highly nonlocal. To isolate the local and nonlocal parts of the pressure, the Poisson equation is used to express the trace of the Hessian in terms of the local velocity gradients, and Equation 7 can be rewritten as

$$\frac{dA_{ij}}{dt} = -\left(A_{ik}A_{kj} - \frac{1}{3}A_{mk}A_{km}\delta_{ij}\right) + H_{ij}^{p} + H_{ij}^{\nu}, \tag{8}$$



Annu. Rev. Fluid Mech. 2011.43:219-245. Downloaded from www.annualreviews.org
by JOHNS HOPKINS UNIVERSITY on 03/17/11. For personal use only.

where

$$H_{ij}^{p} = -\left(\frac{\partial^2 p}{\partial x_i \partial x_j} - \frac{1}{3}\nabla^2 p \delta_{ij}\right) \quad \text{and} \quad H_{ij}^{v} = \nu \frac{\partial^2 A_{ij}}{\partial x_k \partial x_k} \tag{9}$$

are the anisotropic (trace-free) part of the pressure Hessian and the viscous term, respectively. The evolution of $S_{ij}$ and $\Omega_{ij}$ can be obtained from the symmetric and antisymmetric parts of this equation (see, e.g., Nomura & Post 1998 and Tsinober 2009 for detailed discussions).

The evolution equation for the coarse-grained velocity gradient tensor $\tilde{\mathbf{A}}$ is essentially the same (Borue & Orszag 1998, Van der Bos et al. 2002), except that an additional term is added, the gradient of the subfilter force, $H_{ij}^{\tau} = -\partial_j \partial_k \tau_{ik}$, that arises from the effects of scales that have been eliminated through filtering and are represented in the coarse-grained momentum equation through the subgrid or subfilter stress tensor $\widetilde{u_i u_j} - \tilde{u}_i \tilde{u}_j$. Equation 8 is a set of nine coupled, nonlinear, ODEs requiring models for $H_{ij}^{p}$ and $H_{ij}^{v}$.

The wealth of geometric, statistical, and dynamical turbulence phenomena that are accessible through the velocity gradient tensor, together with the fact that an interesting and nontrivial dynamical equation (even though unclosed) is available from the Navier-Stokes equations, makes **A** a dynamical quantity of considerable interest for study in turbulence. Moreover, many practically important phenomena in turbulence, such as growth of lines and surfaces, stretching and quenching of flame surfaces in reacting flows, collision probabilities of particle pairs in the formation of rain drops, and cavitation events, can be strongly affected by the properties of the velocity gradient tensor.

## 2. RESTRICTED EULER EQUATION AND TRACE DYNAMICS

It is instructive to begin by considering the simplest case in which the unclosed terms in Equation 8 are simply not included. This leads to the so-called restricted Euler (RE) system, which is obtained formally by starting from the Euler equations (i.e., setting $\nu = 0$ and thus $H_{ij}^{v} = 0$) and neglecting the anisotropic portion of the pressure Hessian tensor, i.e., $H_{ij}^{p} = 0$ (and $H_{ij}^{\tau} = 0$ in the case of the coarse-grained velocity gradient). This model system was studied in pioneering analytical work by Vieillefosse (1982, 1984) and had been studied in an early numerical experiment by Léorat (1975). Neglecting the anisotropic pressure Hessian amounts to assuming that locally the pressure field surrounding the point of interest is linear, and if it contains quadratic terms in displacement, they are spherically symmetric, e.g., $p(\mathbf{x}) = p(\mathbf{x}_0) + \nabla p \cdot (\mathbf{x} - \mathbf{x}_0) - Q|\mathbf{x} - \mathbf{x}_0|^2$. The RE system can be written as an autonomous dynamical system

$$\frac{dA_{ij}}{dt} + A_{ik}A_{kj} - \frac{1}{3}A_{mn}A_{nm}\delta_{ij} = 0. \tag{10}$$

This set of ODEs is now closed, the time evolution of **A** being fully determined by its initial condition $\mathbf{A}(t_0)$. However, and not unlike the scalar equation $dy/dt - y^2 = 0$, which has a solution with a finite-time singularity $y(t) \sim (t_\infty - t)^{-1}$, the full solution for the tensor $A_{ij}$ can be shown to exhibit such a finite-time singularity for all initial conditions (Vieillefosse 1982) [except for when $Q(t_0) = -[\frac{27}{4}R(t_0)^2]^{1/3}$ and $R(t_0) < 0$, which vanish at long times].

### 2.1. Restricted Euler Dynamics of Scalar Invariants

By multiplication of Equation 10 by $A_{ji}$ and $A_{jk}A_{ki}$, a pair of simple evolution equations for $Q$ and $R$ can be obtained (Vieillefosse 1982, 1984):

$$\frac{dQ}{dt} = -3R, \quad \frac{dR}{dt} = \frac{2}{3}Q^2. \tag{11}$$



Annu. Rev. Fluid Mech. 2011.43:219-245. Downloaded from www.annualreviews.org
by JOHNS HOPKINS UNIVERSITY on 03/17/11. For personal use only.

Annu. Rev. Fluid Mech. 2011.43:219-245. Downloaded from www.annualreviews.org
by JOHNS HOPKINS UNIVERSITY on 03/17/11. For personal use only.

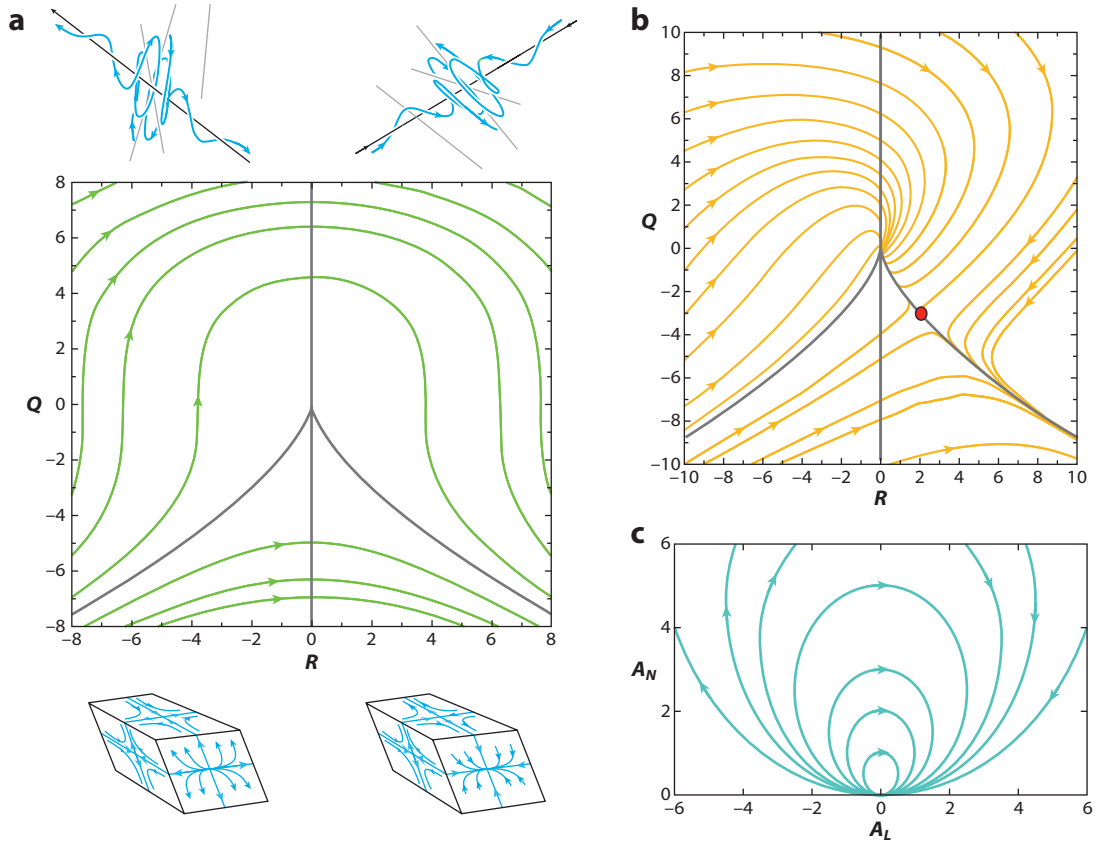


**Figure 3**

(*a*) Phase-space portrait of the restricted Euler model in the *R*, *Q* plane, together with sketches of the local flow topology prevalent in each quadrant. Figure adapted from Martin et al. (1998b) and Ooi et al. (1999). (*b*) Phase-space portrait of the restricted Euler system with linear damping. The red point indicates the unstable saddle. Figure taken from Martin et al. (1998b). (*c*) The $A_L, A_N$ phase diagram for the advected delta-vee system for $Q = 0$. Figure taken from Li & Meneveau (2005).

In the derivation, the Cayley-Hamilton theorem ($A_{im}A_{mn}A_{nj} + QA_{ij} + R\delta_{ij} = 0$, for the case $A_{ii} = 0$) is used to express $\mathbf{A}^3$ in terms of $\mathbf{A}$ and the invariants $Q$ and $R$ themselves. Remarkably, the invariants $R$ and $Q$ uncouple from the other invariants and tensor elements. Eliminating $dt$ and solving for $Q$ as a function of $R$, one sees that there is a time invariant of the RE dynamics, the discriminant $\frac{27}{4}R(t)^2 + Q(t)^3$. It is often denoted as $Q_0^3$, equal to the value of $Q^3$ when $R = 0$. The phase-space flow of this simple dynamical system (Equation 11) is shown in **Figure 3*a***.

The system naturally evolves initial conditions from left to right, and at large times, when $R \to \infty$, the system tends to an $Q \to -\frac{3}{2^{2/3}}R^{2/3}$ asymptote. The units of the system involve only timescales, and thus everything is determined by the initial condition. Cantwell (1992) showed that a natural timescale can be formed from the invariant $Q_0$ according to $t_* \equiv |Q_0|^{-1/2}$ (for $Q_0 \neq 0$). The nondimensional variables $r = Rt_*^3$, $q = Qt_*^2$, $a_{ij} = t_*A_{ij}$, and $\tau = t/t_*$ can thus be defined. When $Q_0 = 0$, one can replace $Q_0$ with the initial value of $Q$ in the definition of $t_*$ (Cantwell 1992). The discriminant becomes $27r^2/4 + q^3 = \mathrm{sgn}(Q_0)$ and can thus take only three values, $\pm 1$ and 0. The upper half of the dynamics (for $Q_0 > 0$) correspond to rotation-dominated dynamics in which two of the three eigenvalues of $\mathbf{A}$ are a complex conjugate pair. For $Q_0 < 0$, the motion

is strain dominated with three real eigenvalues. Further details about topological properties and classifications can be found in Perry & Chong (1987) and Chong et al. (1990).

The evolution equations for the other three invariants that complete the description of the intrinsic structure of the velocity gradient tensor can be similarly derived (Martin et al. 1998b):

$$\frac{dQ_S}{dt} = -2R_S - R, \quad \frac{dR_S}{dt} = \frac{2}{3}QQ_S + \frac{1}{4}V^2, \quad \frac{dV^2}{dt} = -\frac{16}{3}(R_S - R)Q. \tag{12}$$

Together with Equation 11, this defines a dynamical system in 5D phase space. Properties of the system were reported by Martin et al. (1998b), and recently a general fixed-point analysis was performed by Bikkani & Girimaji (2007).

Using DNS data, Lüthi et al. (2009) have shown that a 3D phase-space projection of the 5D phase space, consisting of $Q$, and two variables proportional to $R_S - R$ and $R_S$, can be used for highly insightful data analysis.

There exists another set of scalar invariants whose dynamics uncouple from the full system in an interesting way. This decoupling occurs (Li & Meneveau 2005, 2006) when considering the velocity gradient tensor in a direction represented by the material line with unit vector $\hat{\boldsymbol{\ell}}(t) = \boldsymbol{\ell}/||\boldsymbol{\ell}||$. The material line element $\boldsymbol{\ell}$ obeys the local kinematic condition $d\ell_i/dt = A_{ij}\ell_j$. Two additional scalar quantities are needed to describe the intrinsic structure of the $\mathbf{A} - \hat{\boldsymbol{\ell}}$ configuration as the orientation of $\hat{\boldsymbol{\ell}}$ needs to be described. With respect to $\hat{\boldsymbol{\ell}}$, a longitudinal gradient component can be defined according to $A_L \equiv A_{mn}\hat{\ell}_n\hat{\ell}_m$, representing the change of the velocity component in the $\hat{\ell}$ direction along this same direction. The gradient along $\hat{\boldsymbol{\ell}}$ of the remaining two transverse velocity components can be described through its magnitude according to $A_N^2 \equiv [(\delta_{ik} - \hat{\ell}_i\hat{\ell}_k)A_{kn}\hat{\ell}_n]^2$. Taking the time derivatives of $A_L = A_{mn}\hat{\ell}_n\hat{\ell}_m$ and $A_N$, in combination with Equation 10 and $d\ell_i/dt = A_{ij}\ell_j$, the following pair of equations can be derived (Li & Meneveau 2005):

$$\frac{dA_L}{dt} = -A_L^2 + A_N^2 - \frac{2}{3}Q, \quad \frac{dA_N}{dt} = -2A_LA_N. \tag{13}$$

Together with Equation 11, this forms a 4D system for ($A_L$, $A_N$, $Q$, $R$). For $Q = 0$, the phase-space diagram is shown in **Figure 3*c***. An ad hoc assumption to achieve a further simplification was proposed by Li & Meneveau (2006) that uncouples the dynamics of ($A_L$, $A_N$) from those of ($R$, $Q$): Recognizing that $Q = -A_L^2 + Q^-$, where $Q^-$ are gradients in other directions that cannot be uniquely expressed in terms of ($A_L$, $A_N$), and setting $Q^- = 0$, in 3D turbulence the system simplifies to

$$\frac{dA_L}{dt} = -\frac{1}{3}A_L^2 + A_N^2, \quad \frac{dA_N}{dt} = -2A_LA_N, \tag{14}$$

and is characterized by a time-invariant $U = (A_L^2 + \frac{3}{5}A_N^2)A_N^{-1/3}$. This system was written by Li & Meneveau (2006) for velocity increments and thus was termed the advected delta-vee system. The authors studied the system in detail, including generalizations to arbitrary space dimensions, as well as passive scalar increments or gradients. The system illustrates quite naturally the origin of skewness in the longitudinal gradient, with the self-stretching term $-A_L^2$ on the right-hand side of the equation for $dA_L/dt$ leading to rapid growth in the magnitude of negative gradients, whereas positive gradients decrease in magnitude. Conversely, the origin of very large values of transverse increments (intermittency) can be traced to their rapid growth when $A_L < 0$, in the right-hand side of the equation for $dA_N/dt$. As shown by Galanti et al. (1997), another pair of such variables can be introduced obeying a similar equation, namely the pair $\alpha^* = \boldsymbol{\omega}\cdot\mathbf{S}\cdot\boldsymbol{\omega}/\omega^2$ and $\chi^* = \boldsymbol{\omega}\times\mathbf{S}\cdot\boldsymbol{\omega}/\omega^2$ related to vorticity-vortex stretching alignments. Gibbon & Holm (2007) examined the mathematical structure of variables in more generalized Lagrangian frames. Generalizations including active scalar increments have been studied by Festa et al. (2007).

Annu. Rev. Fluid Mech. 2011.43:219-245. Downloaded from www.annualreviews.org
by JOHNS HOPKINS UNIVERSITY on 03/17/11. For personal use only.

## 2.2. Restricted Euler Solution for the Full Velocity Gradient Tensor

The prior section reviews the dynamics of scalar invariants that lead to simplified descriptions of RE dynamics. It turns out that an analytical solution can be obtained for the full velocity gradient tensor as a function of time. This solution was obtained by Cantwell (1992) by taking the time derivative of Equation 10. Using again the Cayley-Hamilton theorem, one sees that the cubic terms arising from evaluating $d[A_{ik}A_{kj}]/dt$ are simply proportional to $A_{ij}$, i.e., the same indices of the second time derivative being evaluated. Written in its dimensionless form, the result for $a_{ij}(\tau)$ reads (Cantwell 1992)

$$\frac{d^2a_{ij}}{d\tau^2} + \frac{2}{3}q(\tau)a_{ij} = 0. \tag{15}$$

A solution can be obtained by replacing $\tau$ with the time-like variable $s = (3\sqrt{3}/2)r(\tau)$:

$$[\mathrm{sgn}(Q_0) - s^2]\frac{d^2a_{ij}}{ds^2} - \frac{4}{3}s\frac{da_{ij}}{ds} + \frac{2}{9}a_{ij} = 0. \tag{16}$$

This equation can be solved (Cantwell 1992) using hypergeometric functions by a further change of variables, $x = 1 - s^2$ for $Q_0 > 0$ and $x = 1 + s^2$ for $Q_0 < 0$. Cantwell (1992) showed that the solution can be written as a linear combination of two scalar functions of $r$:

$$a_{ij}(\tau) = c_{ij}f_1(r(\tau)) + d_{ij}f_2(r(\tau)), \tag{17}$$

where the constants of integration are given by the initial conditions $a_{ij}(0)$ according to

$$c_{ij} = a_{ij}(0)q_0^2 f_2'(r_0) + \left(\frac{3}{2}a_{ik}(0)a_{kj}(0) + q_0\delta_{ij}\right) f_2(r_0), \tag{18}$$

$$d_{ij} = -a_{ij}(0)q_0^2 f_1'(r_0) - \left(\frac{3}{2}a_{ik}(0)a_{kj}(0) + q_0\delta_{ij}\right) f_1(r_0), \tag{19}$$

where the prime denotes differentiation with respect to $r$. The expressions for $f_1$ and $f_2$ differ for the different types of initial conditions and are denoted by $\pm$ or 0 superscripts. For $Q_0 > 0$ they are

$$f_1^+(r) = \frac{1}{2}\left[b(r)^{\frac{1}{3}} + k(r)^{\frac{1}{3}}\right], \quad f_2^+(r) = \frac{1}{\sqrt{3}}\left[b(r)^{\frac{1}{3}} - k(r)^{\frac{1}{3}}\right], \tag{20}$$

where $b(r) = 1 + \frac{3\sqrt{3}}{2}r$ and $k(r) = 1 - \frac{3\sqrt{3}}{2}r$. When $Q_0 < 0$,

$$f_1^-(r) = \left(1 + \frac{27}{4}r^2\right)^{\frac{1}{6}}\cos\theta, \quad f_1^-(r) = \frac{2}{\sqrt{3}}\left(1 + \frac{27}{4}r^2\right)^{\frac{1}{6}}\sin\theta, \tag{21}$$

where $\theta = \frac{1}{3}\tan^{-1}(\frac{3\sqrt{3}r}{2})$. When $Q_0 = 0$, $f_1^0(r) = 2^{\frac{1}{3}}[\frac{3\sqrt{3}}{2}r]^{-\frac{2}{3}}$ and $f_2^0(r) = \frac{2^{2/3}}{3\sqrt{3}}[\frac{3\sqrt{3}}{2}r]^{\frac{1}{3}}$. The time dependence of these solutions requires the solution of $r(\tau)$. This also was obtained by Cantwell (1992) by solving the trace dynamics given in Equation 11 analytically. Eliminating $r(\tau)$ from the two equations, one obtains an equation for $q(\tau)$, whose solution can be written as an implicit function of $\tau$, and using the discriminant, $r(\tau)$ can be obtained. The initial value of the time variable $\tau$ must be given in terms of the solution itself using the initial values $q_0$ and/or $r_0$. In practice, numerical evaluations require evaluating hypergeometric functions, so a more practical approach is to obtain $r(\tau)$ from careful numerical integration of the two ODEs for $(r(\tau), q(\tau)$ for the three cases $sign(Q_0) = -1, 0, 1)$ and insertion of the solutions into Equations 17–21. Cantwell (1992, figure 2) and Nomura & Post (1998, figure 1) showed some representative time histories of individual velocity gradient tensor elements. Depending on the initial condition, they are characterized by a few variations and then a rapid divergence in finite time.

Annu. Rev. Fluid Mech. 2011.43:219-245. Downloaded from www.annualreviews.org
by JOHNS HOPKINS UNIVERSITY on 03/17/11. For personal use only.

Of interest in Cantwell's solution is the structure of the tensors as the singularity $r \to \infty$ is approached. The predicted structure of the velocity gradient tensor shows a tendency to axisymmetric extension as well as vorticity vector tilting toward the intermediate eigendirection of the strain rate, consistent with the empirical observations summarized in Section 1. Another prediction of the RE dynamics is that the vorticity and strain rate diverge in a similar manner, together. These results hold except for the zero-measure initial condition when it lies precisely on the left branch of the Vieillefosse tail $Q_0 = 0$ and $R(0) < 0$, when the solution tends to zero.

In subsequent work, Cantwell (2002) has shown that, with respect to a redefined time $dt_b = f(t)dt$, a new tensor $b_{ij} = f^{-1}a_{ij}$ can be defined, obeying the RE equation. Although $b_{ij}(t_b)$ displays singularities, the function $f(t)$ can be chosen in such a way that the singularity is relegated to infinite time. The ability to change the system in this form is interesting although the relationship between the redefined timescale and real time remains ad hoc. Another variant of RE dynamics that includes a Reynolds decomposition, treating the mean and fluctuating gradients separately, has been studied by Girimaji & Speziale (1995).

Before turning our attention to the various approaches that have been proposed to counteract the finite-time singularity that arises from RE, we discuss the evolution of fluid elements. Properties of the geometry of fluid elements play a central role in various phenomenological models described in Section 3.

## 2.3. Restricted Euler and Material Deformation

The Lagrangian evolution of material elements has been extensively studied in various works (e.g., Batchelor 1952, Cocke 1969, Girimaji & Pope 1990b, Goto & Kida 2002, Guala et al. 2005). A description of material finite deformation in a continuum is done conveniently using the deformation tensor defined according to $D_{ij}(\mathbf{X}, t) = \partial x_i / \partial X_j$, where $x_i(\mathbf{X}, t)$ denotes the position at time $t$ of a fluid particle that was at the position $x_i(\mathbf{X}, t_0) = X_i$ at the initial time $t_0$. $D_{ij}$ thus describes the variation of the position of a particle at the current time when one slightly changes the initial position. The fluid particle obeys $dx_i/dt = u_i(\mathbf{x}, t)$, and differentiating this expression with respect to $X_j$, one obtains the evolution equation for $D_{ij}$:

$$\frac{dD_{ij}}{dt} = A_{ik}D_{kj}. \tag{22}$$

Nondimensionalizing as in Section 2.2, taking the time derivative of the above equation, and using RE dynamics to describe the time evolution of the velocity gradient tensor, Li & Meneveau (2007) noticed that

$$\frac{d^2D_{ij}}{d\tau^2} = a_{ik}a_{kl}D_{lj} + \left(-a_{ik}a_{kl} - \frac{2}{3}q(\tau)\delta_{il}\right)D_{lj} = -\frac{2}{3}q(\tau)D_{ij}. \tag{23}$$

Comparing Equation 23 with Equation 15, it is apparent that in RE dynamics $D_{ij}$ obeys the same equation as $a_{ij}$. Therefore, the RE solution method of Cantwell (1992) can also be applied to this equation. The coefficients depending on the initial conditions differ from those for $a_{ij}$ because now $D_{ij}(t_0) = \delta_{ij}$ and $dD_{ij}(t_0)/d\tau = a_{ij}(t_0)$, as shown by Li & Meneveau (2007). Once the analytical solution has been obtained, the corresponding Cauchy-Green tensor can be obtained from its definition according to $C_{ij} = D_{ik}D_{jk}$. **Figure 4** shows a comparison of the evolution of material volumes as evaluated from DNS and from the analytical RE solution. Spheres are placed at some initial points in the flow along four lines on two planes. Fluid trajectories originating there are shown as lines. The DNS is used to evaluate the evolution of the Cauchy-Green tensor along this trajectory, and the analytical model based on RE is also evaluated along the trajectory using only the initial condition. As seen in **Figure 4** for short times, there is good agreement



Annu. Rev. Fluid Mech. 2011.43:219-245. Downloaded from www.annualreviews.org
by JOHNS HOPKINS UNIVERSITY on 03/17/11. For personal use only.

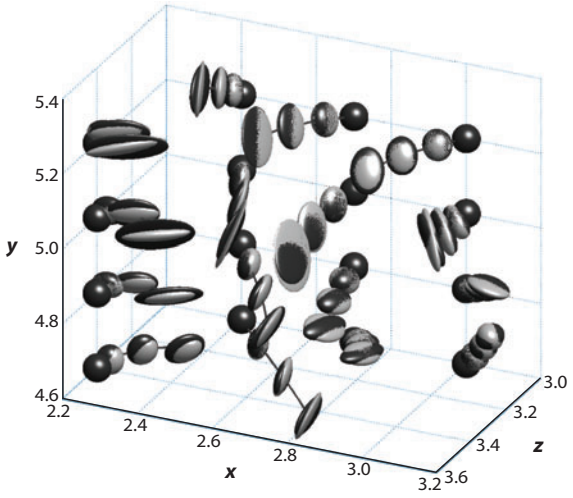


**Figure 4**

Short time evolution of material elements from spheres into ellipsoids along several fluid particle trajectories. The ellipsoids are defined based on the eigenvectors and eigenvalues of the Cauchy-Green tensor. Snapshots along trajectories at $t = 0.5\tau_K$, $1\tau_K$, and $1.5\tau_K$ are shown, starting from spheres at $t = 0$. Lines represent the trajectories of the centers of the material elements, calculated from direct numerical simulation (DNS) data. The dark ellipsoids represent DNS data, whereas light ellipsoids represent the analytic solution obtained with reduced Euler approximation. Figure adapted from Li & Meneveau (2007).

(Li & Meneveau 2007). In almost all the cases, however, the spheres become pancake-like too quickly. The finite-time singularity follows this excessive flattening, and the material elements typically reach zero thickness in finite time. Among others, models for the pressure Hessian and viscous terms described in the next section aim at weakening this excessively strong trend to flatten material elements.

## 3. LAGRANGIAN MODELS FOR THE VELOCITY GRADIENT TENSOR

The goal of the models reviewed in this section is to supplement the RE dynamics with additional terms that represent the discarded physics contained in the deviatoric part of the pressure Hessian $H_{ij}^{p}$ and in the viscous term $H_{ij}^{v}$. The hope is that, if models contain a realistic representation of these terms, then the finite-time singularity could be avoided for arbitrary initial conditions, and also that statistically stationary and realistic dynamics that do not decay to zero may be produced and that time series of $A_{ij}(t)$ approximate those observed in real turbulence.

### 3.1. The Linear Damping Model

The simplest way to try to counteract the finite-time singularity is to add a linear damping. This approach, studied in detail by Martin et al. (1998a), is equivalent to assuming that $H_{ij}^{p} + H_{ij}^{v} = -\tau_0^{-1} A_{ij}$, where $\tau_0$ is a relaxation timescale. Because the term is linear, each of the equations for the invariants given in Equations 11 and 12 $dY/dt = \cdots$ (for $Y = R, Q, R_S, Q_S$, or $V^2$) also inherits an additional damping term $-bY/\tau_0$, with $b = (3, 2, 3, 2, 4)$ in equations for $R$, $Q$, $R_S$, $Q_S$, $V^2$, respectively. It was quickly realized, however, that such linear damping would not be sufficient to avoid the singularity for all initial conditions. Linear damping can lead to exponential reduction of the solution, but this cannot compete with the growth associated with an algebraic finite-time



Annu. Rev. Fluid Mech. 2011.43:219-245. Downloaded from www.annualreviews.org
by JOHNS HOPKINS UNIVERSITY on 03/17/11. For personal use only.

singularity. **Figure 3*b*** shows the trajectories in the phase space of the system $\dot{Q} = -3R - 2Q/\tau_0$, $\dot{R} = \frac{2}{3}Q^2 - 3R/\tau_0$ (Martin et al. 1998a). As is evident, the origin has become a stable node, with a basin of attraction encompassing the trajectories originating above the separatrix (and below the top one—not shown in the figure). However, a saddle point appears at $(R, Q) = (2\tau_0^{-3}, -3\tau_0^{-2})$, and for initial conditions falling outside the basin of attraction of the origin, the solution still diverges. Martin et al. (1998a) performed Monte-Carlo simulations starting the system from a large ensemble of initial conditions and evolved the system in time. They showed that there are (intermediate) times when some quasi-stationary conditions may be reached. During these intermediate times, they found the trends characteristic of the RE system, i.e., the inherent features of the velocity gradient tensor: alignment of the vorticity with intermediate eigendirection and prevalence of axisymmetric extension. However, ultimately solutions either are damped toward the origin or succumb to the finite-time singularity.

We remark that data suggest that a linear damping model may be a good approximation for the viscous term (see the discussion below in Section 3.6), but it does not at all represent the effects of the pressure Hessian, which, instead of relaxing solutions toward the origin, tends to oppose the RE flow in the $R > 0$, $Q < 0$ quadrant but displays more complicated trends in the other quadrants, as discussed by Ooi et al. (1999), Chevillard et al. (2008), and Lüthi et al. (2009).

## 3.2. Stochastic Diffusion Model with Prescribed Log-Normal Dissipation

An early effort to provide a consolidated model for $H_{ij}^{p}$ and $H_{ij}^{v}$ was undertaken by Girimaji & Pope (1990a). The essential ingredient is the addition of a stochastic term, and thus the equation is written as a stochastic differential equation as

$$dA_{ij} = (-N_{ij} + M_{ij})dt + D_{ijkl}dW_{kl}, \tag{24}$$

where the drift coefficient $(-N_{ij} + M_{ij})$ contains a deterministic part $N_{ij} = A_{ik}A_{kj} - \frac{1}{3}A_{mn}A_{nm}\delta_{ij}$ from the RE self-interaction term, and $M_{ij}$ is an additional drift term meant to model parts of the deviatoric part of the pressure Hessian. The tensor $D_{ijkl}$ is the diffusion coefficient, modulating $dW_{lk}$, a tensor-valued Wiener process with zero mean $\langle dW_{kl}\rangle = 0$ and prescribed isotropic unit variance $\langle dW_{pq}dW_{kl}\rangle = \delta_{pk}\delta_{ql}dt$. To determine $M_{ij}$ and $D_{ijkl}$, Girimaji & Pope (1990a) followed an approach often used in PDF methods, namely to use moment constraints and choose model terms so that the system will, by construction, provide certain known behaviors and statistical moments. They chose the well-known log-normal statistics of the dissipation rate as an imposed constraint. They used the pseudodissipation $\epsilon' = \nu A_{mn}A_{mn}$, which is more conveniently expressed in terms of **A**. Building on an existing log-normal Uhlenbeck-Ornstein process as a model for log-normal dissipation rate (Pope & Chen 1990), the authors showed that a drift term of the form

$$M_{ij} = -A_{ij}\left(\frac{1}{2\tau_k}\ln(A_{mn}A_{mn}) - \frac{A_{lk}N_{lk}}{A_{mn}A_{mn}} + \frac{7}{2}\hat{a}^2\right) \tag{25}$$

will generate, for the contraction $A_{mn}A_{mn}$, a diffusion process with log-normal statistics and prescribed variance of the logarithm equal to $\sigma^2$. The value of $\hat{a}^2 = \sigma^2/2\tau_K$ allows this to be specified. The diffusion coefficient is given by

$$D_{ijkl} = \hat{a}\sqrt{A_{mn}A_{mn}}\left(\delta_{ik}\delta_{jl} - \frac{1}{3}\delta_{ij}\delta_{kl}\right). \tag{26}$$

Girimaji & Pope (1990a) tested several variants of this model and showed that, unlike the linear damping model without forcing, this model does generate stationary statistics by virtue of the additional drift terms that diagnose and counteract the growth of $A_{mn}A_{mn}$ and thus prevent the



Annu. Rev. Fluid Mech. 2011.43:219-245. Downloaded from www.annualreviews.org
by JOHNS HOPKINS UNIVERSITY on 03/17/11. For personal use only.

unbounded growth of **A**. Collapse to the origin is prevented through the stochastic forcing. Comparison of the predicted statistical moments of several velocity gradient invariants with results from moderate–Reynolds number DNS showed, however, that an additional tensor $L_{ij}$ needed to be included in the drift term to produce more realistic moments. The predicted (stationary) joint PDF of $R$ and $Q$, the vorticity strain-rate alignment, and the high probability of axisymmetric extension are all quite realistic (at the Reynolds number that was tested), owing to the noticeable effects of the exact $N_{ij}$ term in the model. However, the approach must assume prior knowledge of some of the moments and statistics of **A** and is not based on any physically motivated model of the pressure Hessian or viscous terms. She et al. (1991) described another early attempt to add stochastic terms to the equation, by modeling the pressure Hessian as a random matrix.

### 3.3. The Tetrad Model

The tetrad model was proposed by Chertkov et al. (1999) and is based on a particle representation of the velocity at four fluid particles that form a tetrad. The relative particle locations define a triplet of vector displacements $\boldsymbol{\rho}_a(t)$ $(a = 1, 2, 3)$, which may be written as a $3 \times 3$ matrix. This description has physical appeal as it relates to directly measurable particle locations in turbulent flows and enables an informative visualization of the tetrad as it is being advected and deformed. Chertkov et al. (1999) introduced a decomposition of the local velocity field into a coarse-grained part and a stochastic part that would correspond to incoherent small-scale motions. The coarse-grained velocity gradient tensor, which they denote as **M**, is similar to the filtered coarse-grained tensor $\tilde{\mathbf{A}}$ defined above, except that for the latter a time-independent filter scale is used, whereas the length scale at which **M** is defined depends intrinsically on the time evolution of the relative displacements. Chertkov et al. (1999) arrived at similar evolution equations for **M** and $\boldsymbol{\rho}$ as that for $\tilde{\mathbf{A}}$ and the deformation tensor **D**, the latter having been derived using Cartesian coordinates and gradient, instead of the tetrad displacement vectors. Defining a symmetric moment of inertia tensor $\mathbf{g} = \boldsymbol{\rho}^T \boldsymbol{\rho}$ (similar to the Cauchy-Green tensor **C** defined in Section 2.3), and now following the formulation as given by Naso & Pumir (2005), the tetrad model's dynamical evolution is written as

$$\frac{dM_{ij}}{dt} + (1-\alpha)(M_{ik}M_{kj} - \Pi_{ij}M_{mn}M_{nm}) = \eta_{ij}, \tag{27}$$

$$\frac{dg_{ij}}{dt} - g_{ik}M_{kj} - g_{jk}M_{ki} - \beta\sqrt{M_{mn}M_{mn}}\left(g_{ij} - \frac{1}{3}g_{kk}\delta_{ij}\right) = 0. \tag{28}$$

The tensor $\Pi_{ij}$ can be thought of as proportional to the pressure Hessian nondimensionalized using $M_{mn}M_{mn}$. A stochastic forcing term $\eta_{ij}$ is added. It is specified to be Gaussian, white in time, and complying with Kolmogorov scaling with respect to the scale in question. The other term $\alpha(M_{ik}M_{kj} - \Pi_{ij}M_{mn}M_{nm})$, with $0 < \alpha < 1$, opposes the deterministic RE dynamics and is motivated by DNS results of Borue & Orszag (1998). Note that with $\alpha = 1$ the RE self-stretching dynamics are entirely canceled.

A crucial element in the tetrad model is the ability to use the geometry of the tetrad as embodied by $\boldsymbol{\rho}$ or **g** in modeling the pressure Hessian using the tensor $\Pi_{ij}$. Considering the time evolution of the local kinetic energy of velocity increments over the tetrad (which can be expressed in terms of $\boldsymbol{\rho}$ and **M**), Chertkov et al. (1999) showed that the following form does not affect the kinetic energy and thus may be appropriate as a model for the kinetic energy–conserving nonlinear term in the Navier-Stokes equation:

$$\Pi_{ij} = \frac{(\mathbf{g}^{-1})_{ij}}{(\mathbf{g}^{-1})_{kk}}. \tag{29}$$



Annu. Rev. Fluid Mech. 2011.43:219-245. Downloaded from www.annualreviews.org
by JOHNS HOPKINS UNIVERSITY on 03/17/11. For personal use only.

RE is recovered for undeformed tetrads for which $\Pi_{ij} = \delta_{ij}/3$. Besides the conservation of kinetic energy, Chertkov et al. (1999) pointed out that such an expression measures the overall deformation of the tetrad. As it becomes more deformed, it acts to oppose further deformation of the tetrad and may thus counteract the singularity-forming trend of RE dynamics. As shown in Section 3.5, Equation 29 can also be interpreted as a closure for the pressure Hessian when it is assumed that its Lagrangian pre-image is an isotropic tensor.

Chertkov et al. (1999) analyzed the Fokker-Planck equation for the joint PDF $f(\mathbf{M}, \boldsymbol{\rho})$ corresponding to the model. The physical and geometric picture encoded in the system is that initially isotropic tetrads, at the turbulence integral scale, evolve in time under the action of the deterministic RE dynamics and the stochastic forcing terms. They grow in some directions and shrink in others. The smallest characteristic scale of the evolving tetrad can be understood as the scale at which the velocity gradient is defined; i.e., one is following the Lagrangian evolution of the cascade.

The basic tool used by Chertkov et al. (1999) to analyze the model system involves path-integral methods applied to the PDF equation. For a specified final configuration of the tetrad and of velocity gradients, the desired probability $f(\mathbf{M}, \boldsymbol{\rho})$ is evaluated by integrating backward in time and using as the initial condition the Gaussianity of the velocity gradients at integral scales. To evaluate integrals over all possible initial conditions, the authors used saddle-point approximations and coupled the approach with Monte-Carlo simulations (the hybrid method). The results were compared with DNS results. **Figure 5** shows the predicted joint PDF of $R$ and $Q$ at two scales, using the hybrid method. Whereas at integral scales $L$ the results are consistent with Gaussian statistics (not shown), at a smaller scale $\ell = L/2$, the Vieillefosse tail and sheared drop shape appear. As time proceeds further, and the length scales become smaller ($\ell = L/4$), some unphysical artifacts may be observed as the probability around the Vieillefosse tail becomes exaggerated, and there is some bulging in the $R > 0$, $Q > 0$ quadrant.

Chertkov et al. (1999) further compared conditional moments of various other interesting quantities, such as the conditional enstrophy $\langle \omega_i \omega_i | R, Q \rangle$ and strain skewness $\langle S_{ik} S_{km} S_{mi} \mid R, Q \rangle$, and showed that the tetrad model predicts many of the trends of such quantities, at least at scales that are not too small. Further variants of the model and applications to cases with mean shear and dispersion have been explored in several subsequent papers (Naso & Pumir 2005; Naso et al. 2006, 2007; Pumir et al. 2000). For a particle-based large-eddy simulation scheme inspired by the tetrad model, the reader is referred to Pumir & Shraiman (2003).

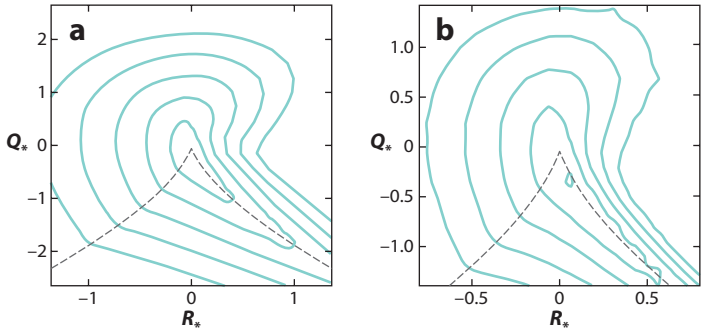


**Figure 5**

Joint probability density function of $R$ and $Q$ predicted by the tetrad model, computed using the hybrid solution method (Naso et al. 2007) for scales (*a*) $r = L/2$ and (*b*) $r = L/4$. Figure adapted from Naso et al. (2007).



Annu. Rev. Fluid Mech. 2011.43:219-245. Downloaded from www.annualreviews.org
by JOHNS HOPKINS UNIVERSITY on 03/17/11. For personal use only.

### 3.4. The Lagrangian Linear Diffusion Model

The Lagrangian linear diffusion model focuses on the unclosed viscous term $\nu\partial^2 A_{ij}/\partial x_k^2$ appearing in the equation for the unfiltered velocity gradient tensor at viscous length scales. As shown by Martin et al. (1998a) (see Section 3.1), a linear closure $\nu\partial^2 A_{ij}/\partial x_k^2 = -A_{ij}/\tau_0$ is not sufficiently strong to counteract the RE-induced finite-time singularity. However, Jeong & Girimaji (2003) proposed to use the Eulerian-Lagrangian change of variables for gradients,

$$\frac{\partial F}{\partial x_k} = \frac{\partial F}{\partial X_m}\frac{\partial X_m}{\partial x_k} = \frac{\partial F}{\partial X_m}(\mathbf{D}^{-1})_{mk}, \tag{30}$$

applied twice. Then the viscous term is modeled according to

$$\nu\frac{\partial^2 A_{ij}}{\partial x_k \partial x_k} \approx \nu(\mathbf{C}^{-1})_{mn}\frac{\partial^2 A_{ij}}{\partial X_m \partial X_n}, \tag{31}$$

where $\mathbf{C} = \mathbf{D}\mathbf{D}^{\mathrm{T}}$ is the Cauchy-Green tensor analogous to the moment of inertia tensor $\mathbf{g}$ used in the tetrad model. They go on to make the isotropy assumption on the Cauchy-Green tensor inverse, i.e., $(\mathbf{C}^{-1})_{mn} \approx \frac{1}{3}\delta_{mn}(\mathbf{C}^{-1})_{kk}$, together with a linear ansatz for the Lagrangian Laplacian, $\nu\partial^2 A_{ij}/\partial X_m^2 \approx -A_{ij}/\tau_L$, and arrive at a Lagrangian linear diffusion model:

$$\frac{dA_{ij}}{dt} + \left(A_{ik}A_{kj} - \frac{1}{3}\delta_{ij}A_{mn}A_{nm}\right) = -\frac{(\mathbf{C}^{-1})_{kk}}{3\tau_L}\left(1 - \frac{\epsilon_s}{A_{mn}A_{mn}}\right). \tag{32}$$

The parameter $\epsilon_s$ is a desired target value for the pseudodissipation $A_{mn}A_{mn}$, and the last term thus provides (deterministic) forcing because in the absence of the nonlinear terms, $A_{ij}$ should relax toward values such that $A_{mn}A_{mn} = \epsilon_s$. The Cauchy-Green tensor $\mathbf{C}$ is obtained from integration of its evolution equation (obtained from Equation 22), which therefore leads to an evolving state without stationary statistics. Without the forcing (or $\epsilon_s = 0$), **Figure 6*a*** shows the typical behavior of trajectories of this system. Unlike the linear diffusion model, and akin to the tetrad model, this approach is able to eliminate the finite-time singularity. With forcing, **Figure 6*b*** shows a scatter plot of the predicted joint PDF of $R$ and $Q$. Again owing to the influence of the RE self-stretching terms, the model displays the preference for ($R$, $Q$) pairs along the Vieillefosse tail, alignment and

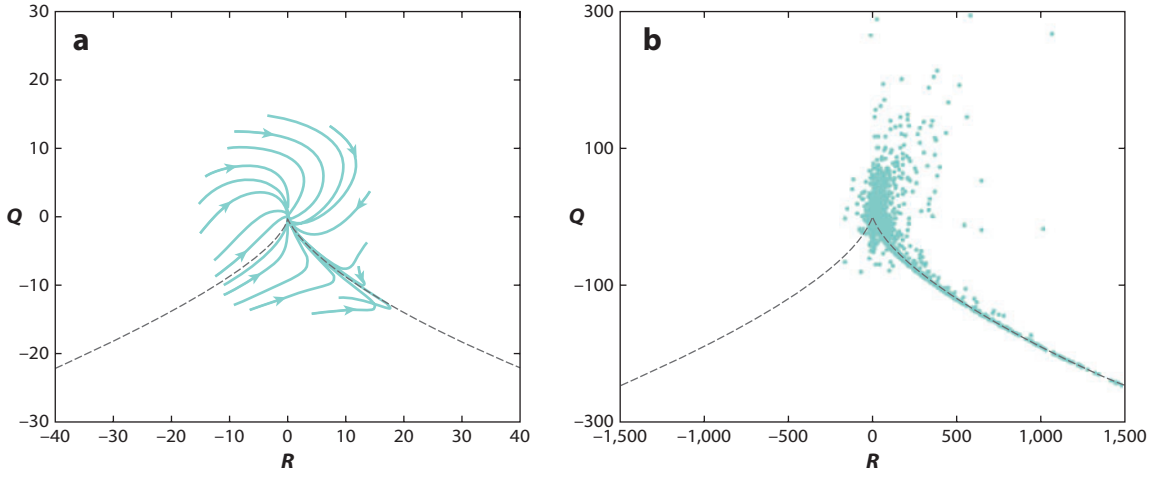


**Figure 6**

(*a*) $R$ and $Q$ phase space for the Lagrangian linear diffusion model of Jeong & Girimaji (2003). (*b*) Scatter plot of $R$ and $Q$ as predicted by the Lagrangian linear diffusion model. Figure adapted with permission from Jeong & Girimaji (2003), copyright 2003, Springer.

Annu. Rev. Fluid Mech. 2011.43:219-245. Downloaded from www.annualreviews.org
by JOHNS HOPKINS UNIVERSITY on 03/17/11. For personal use only.

axisymmetric deformation statistics, and strain skewness. However, as is also the case in the tetrad model, there is a bulging in the $R > 0$, $Q > 0$ quadrant and an excessively pronounced likelihood along the Vieillefosse tail. Similarly, the fluid deformation described by $\mathbf{D}$ keeps evolving in time, so the relevant length scales keep changing.

### 3.5. The Recent Fluid Deformation Approximation

The recent fluid deformation approximation (RFDA) was proposed by Chevillard & Meneveau (2006) and can be considered a simplified version of the Chertkov et al. (1999) tetrad model, with elements of the Lagrangian linear diffusion model of Jeong & Girimaji (2003). A salient feature of the approach is that the dynamical equations for the fluid deformations are not simulated exactly but are heavily modeled. The starting point is an Eulerian-Lagrangian change of variables

$$\frac{\partial^2 p(\mathbf{x},t)}{\partial x_i \partial x_j} \approx \frac{\partial X_m}{\partial x_i}\frac{\partial X_n}{\partial x_j}\frac{\partial^2 p(\mathbf{x},t)}{\partial X_m \partial X_n}, \tag{33}$$

where the approximation arises from neglecting spatial gradients of $\mathbf{D}$. The Lagrangian pressure Hessian $\partial^2 p/\partial X_m \partial X_n$ is modeled based on the assumption that as time progresses, one loses memory about the relative orientations of the initial locations $\mathbf{X}$ as far as the present value of pressure is concerned. Hence, the Lagrangian pressure Hessian is assumed to be isotropic leading to

$$\frac{\partial^2 p}{\partial x_i \partial x_j} \approx \frac{\partial X_m}{\partial x_i}\frac{\partial X_n}{\partial x_j}\frac{1}{3}\delta_{mn}\frac{\partial^2 p}{\partial X_k \partial X_k} = (\mathbf{C}^{-1})_{ij}\frac{1}{3}\frac{\partial^2 p}{\partial X_k \partial X_k}, \tag{34}$$

where $\mathbf{C}$ is again the Cauchy-Green tensor. To determine $\partial^2 p/\partial X_k \partial X_k$, we follow Chertkov et al. (1999) and use the Poisson equation, namely $\nabla^2 p = -A_{nm}A_{mn} = (1/3)(\mathbf{C}^{-1})_{qq}\partial^2 p/\partial X_k \partial X_k$. Solving for $\partial^2 p/\partial X_k \partial X_k$ and replacing it back into Equation 34 lead to

$$\frac{\partial^2 p}{\partial x_i \partial x_j} = -\frac{\mathrm{Tr}(\mathbf{A}^2)}{\mathrm{Tr}(\mathbf{C}^{-1})}(\mathbf{C}^{-1})_{ij} = \frac{2Q}{\mathrm{Tr}(\mathbf{C}^{-1})}(\mathbf{C}^{-1})_{ij}. \tag{35}$$

Recognizing the similarity between the Cauchy-Green tensor $\mathbf{C}$ and the conformation tensor $\mathbf{g}$ used in the tetrad model, we see that Equation 35 is essentially equivalent to the term $\Pi_{ij}\mathrm{Tr}(\mathbf{A}^2)$ entering the tetrad model (see Equation 29). For the viscous term, similar to Jeong & Girimaji (2003), the change of variables is applied to the viscous Laplacian $\nu\nabla^2 A_{ij}$. Furthermore, Chevillard & Meneveau (2006) showed that the appropriate spatial decorrelation length scale is the Taylor microscale $\lambda$, and this leads to the following model for the viscous term:

$$\nu\frac{\partial^2 \mathbf{A}}{\partial x_k \partial x_k} \approx -\frac{1}{T}\frac{\mathrm{Tr}(\mathbf{C}^{-1})}{3}\mathbf{A}, \tag{36}$$

where $T$ is the integral timescale $T = \lambda^2/\nu$.

As it stands, the required Cauchy-Green tensor $\mathbf{C}$ can be obtained from its transport equation subject to the natural initial condition $C_{ij}(t_0) = \delta_{ij}$. Due to turbulence dispersion, $\mathbf{C}$ continues to evolve with exponentially growing and decreasing eigenvalues. In the tetrad model, this is addressed by including a diffusion term in its equation (Equation 28), which relaxes the tensor toward an isotropic one at a timescale proportional to $(A_{mn}A_{mn})^{-1/2}$. Also, one notes that the growing eigenvalues are controlled by the normalization factor $\mathrm{Tr}(\mathbf{C}^{-1})$ from the Poisson equation.

In a sort of Markovianization of the dynamics of $\mathbf{C}$, the RFDA assumes that $\mathbf{C}$ evolves in a frozen velocity gradient field during a characteristic (short) time. The value of $\mathbf{A}$ during that time is taken as the most recent value (i.e., the current, local, value). Moreover, the timescale chosen is the typical decorrelation timescale of $\mathbf{A}$ during its Lagrangian evolution, which is known to be of the order of the Kolmogorov timescale, $\tau_K$ [the timescale $(A_{mn}A_{mn})^{-1/2}$ was also tested].



Annu. Rev. Fluid Mech. 2011.43:219-245. Downloaded from www.annualreviews.org
by JOHNS HOPKINS UNIVERSITY on 03/17/11. For personal use only.

Solving the equation for $\mathbf{D}$ using matrix exponentials and replacing it into the definition of $\mathbf{C}$ yield $\mathbf{C}(t) = exp(\mathbf{A}\tau_K)\mathbf{C}(t-\tau_K)exp(\mathbf{A}^T\tau_K)$. The initial time is taken to be $t-\tau_K$. The upstream, prior value of the Cauchy-Green tensor is assumed to be isotropic and undeformed $C_{ij}(t-\tau_K) = \delta_{ij}$. Thus, in the RFDA, one replaces the true Cauchy-Green tensor by a new tensor, called the recent Cauchy-Green tensor $\mathbf{C}_{\tau_K}$ that can be expressed in terms of simple matrix exponentials:

$$\mathbf{C}_{\tau_K} = e^{\tau_K \mathbf{A}} e^{\tau_K \mathbf{A}^T}. \tag{37}$$

Inserting Equations 35 and 36 into Equation 7 yields

$$dA_{ij} = \left( -A_{ik}A_{kj} + \frac{\mathrm{Tr}(\mathbf{A}^2)}{\mathrm{Tr}(\mathbf{C}_{\tau_K}^{-1})}(\mathbf{C}_{\tau_K}^{-1})_{ij} - \frac{\mathrm{Tr}(\mathbf{C}_{\tau_K}^{-1})}{3T}A_{ij} \right) dt + D_{ijkm}dW_{km}, \tag{38}$$

with $\mathbf{C}_{\tau_K}$ expressed in terms of $\mathbf{A}$ according to Equation 37. Thus, the essential difference between the tetrad model and the RFDA is that in the tetrad model the length scale is evolving in time, and one solves additional ODEs for the geometry, whereas in the RFDA the scale is assumed fixed, and the geometry equation is heavily modeled and simplified.

As in the other stochastic models, the system is forced with a stochastic delta-correlated Gaussian noise $d\mathbf{W}$ (with the right tensor symmetries determined by $\mathbf{D}$). Random forcing has been added to represent possible forcing effects, e.g., from neighboring eddies. The deterministic part of the model involves two timescales: a small timescale $\tau_K$ and a large one $T$. Hence, the deterministic part gives Reynolds number ($Re$) dependence through the ratio $(T/\tau_K)^2 \sim Re$, according to classical Kolmogorov dimensional arguments (Frisch 1995). The model can also be applied for $\tilde{\mathbf{A}}$ in the inertial range, in which case the molecular viscosity can be replaced with an appropriate eddy viscosity as a model for $\mathbf{H}^r$.

## 3.6. Recent Fluid Deformation Approximation Results

The system of stochastic differential equations has been studied in detail through numerical integration by Chevillard & Meneveau (2006, 2007), Chevillard et al. (2008), and Martins-Afonso & Meneveau (2010). Chevillard et al. (2008) presented extensive comparisons with DNS results at moderate Reynolds number $R_\lambda = 150$. The main parameter of the model is the ratio of timescales $\tau_K/T$, related to the Reynolds number. The model is run with $\tau_K/T = 10^{-1}$, which corresponds roughly to the ratio of these timescales in the DNS. **Figures 7*a*,*b*** show a comparison of the predicted joint PDF of $R$ and $Q$ predicted by the model and in the DNS, whereas **Figures 7*c*,*d*** compare the PDF of the cosine of the angle between the vorticity vector and strain-rate eigenvectors. As in the other models that maintain the effects of the nonlinear self-stretching term, these trends are well captured, still with some qualitative differences. Also, Chevillard & Meneveau (2006) showed that the $A_{11}$ third-order moment displays realistic levels of skewness. Further comparisons include conditional averages of enstrophy, strain skewness, and energy transfer $A_{ij}A_{im}A_{jm}$.

Additional insights are provided by analysis of the probability current in the associated Fokker-Planck equation as written for the model and as obtained from evaluation of the conditional statistics of the respective terms in DNS. **Figure 8** displays vector maps and field lines associated with the probability flow, for each of the terms. At the top is the deterministic probability flow from the closed RE dynamics that pushes probabilities toward the right tail of the Vieillefosse line. The results for the pressure Hessian flow are instructive. As remarked by Chevillard et al. (2008), the pressure Hessian counteracts the effects induced by the RE terms as the flux goes toward the center of the RQ plane along the right tail of the Vieillefosse line. This feature is well reproduced by the model, with vector magnitudes of the same order. Another important effect of the pressure Hessian is that in the $R < 0$ left half-plane, the probability current leads the

Annu. Rev. Fluid Mech. 2011.43:219-245. Downloaded from www.annualreviews.org
by JOHNS HOPKINS UNIVERSITY on 03/17/11. For personal use only.

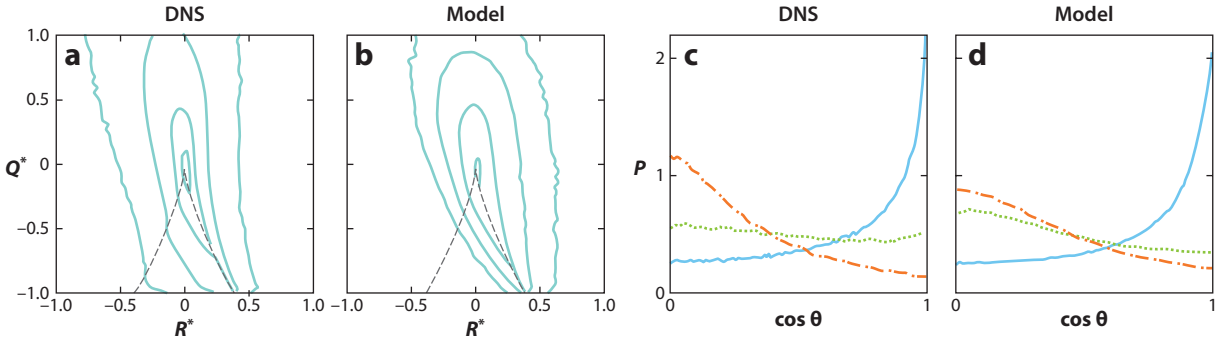


**Figure 7**

Comparison of statistics predicted by the recent fluid deformation approximation stochastic model and direct numerical simulation (DNS) of isotropic turbulence at $R_\lambda = 150$. (*a*,*b*) Joint probability density function (PDF) of $R^*$ and $Q^*$ ($R^* = R/\langle S_{mn}S_{mn}\rangle^{3/2}$ and $Q^* = Q/\langle S_{mn}S_{mn}\rangle$). (*c*,*d*) PDF of cosine of angle between vorticity vector and strain-rate eigenvectors. Figure reproduced from Chevillard et al. (2008).

Annu. Rev. Fluid Mech. 2011.43:219-245. Downloaded from www.annualreviews.org
by JOHNS HOPKINS UNIVERSITY on 03/17/11. For personal use only.

probability toward the left tail of the Vieillefosse line. This feature is evidently not reproduced by the model, which instead appears to act exclusively in the vertical direction, upward in the $Q < 0$ plane and downward in the $Q > 0$ plane. This may explain why the model leads to an underestimation of probability in the bottom-left quadrant and an overprediction of probability of events in the upper-right quadrant. A marked feature of the DNS results is that the magnitudes of the vectors are essentially negligible in the entire vortex contraction quadrant above the right Vieillefosse line, and, unlike in the model, the flow does not vanish on the $Q = 0$ line. As argued by Chevillard et al. (2008), this difference is shared also by interesting, more generalized closures of the pressure Hessian proposed by Gibbon & Holm (2007) in terms of generalized symmetric tensors, as they still require the trace of the tensor to be proportional to $Q$ to conform to the Poisson equation, leading to vanishing flow on the $Q = 0$ line.

For the viscous term, one observes in **Figures 8*e*,*f*** that the model reproduces the probability flux reasonably well. Consistent with the observations already made by Martin et al. (1998b) and Van der Bos et al. (2002), the viscous effect is to push the probabilities toward vanishing $R$ and $Q$, not only along the Vieillefosse line but also everywhere else. **Figures 8*g*,*h*** show the sum of all the terms, the total probability current. For the DNS, it corresponds to the sum of **Figures 8*a*,*c*,*e***. For the RFDA, it also includes the effects of the diffusion term, which must be evaluated from the model runs with special care (see Chevillard et al. 2008, appendix B). The circular motion around the origin of the $R$, $Q$ plane has already been reported by Ooi et al. (1999) and Chertkov et al. (1999).

Martins-Afonso & Meneveau (2010) further analyzed the model by studying simplifications of the matrix exponential in the limit of small $\tau_K/T$ via Taylor-series expansions. They showed that even first-order approximations yield reasonably realistic approximations to the dynamics with the full matrix exponentials, although in some cases some difference persists when the gradients become very large. Attempts to run the models at significantly higher Reynolds numbers (e.g., with $\tau_K/T = 10^{-2}$ and $10^{-3}$), however, have shown degrading results, with unphysical tails developing in the PDFs and other statistical parameters. All the models reviewed above appear to have difficulties in reaching arbitrarily high Reynolds number. This poses difficulties in using such Lagrangian stochastic models to study fundamental properties of scaling with Reynolds number; for instance, the scaling of the flatness of $A_{11}$ as function of Reynolds number is not available through this approach.

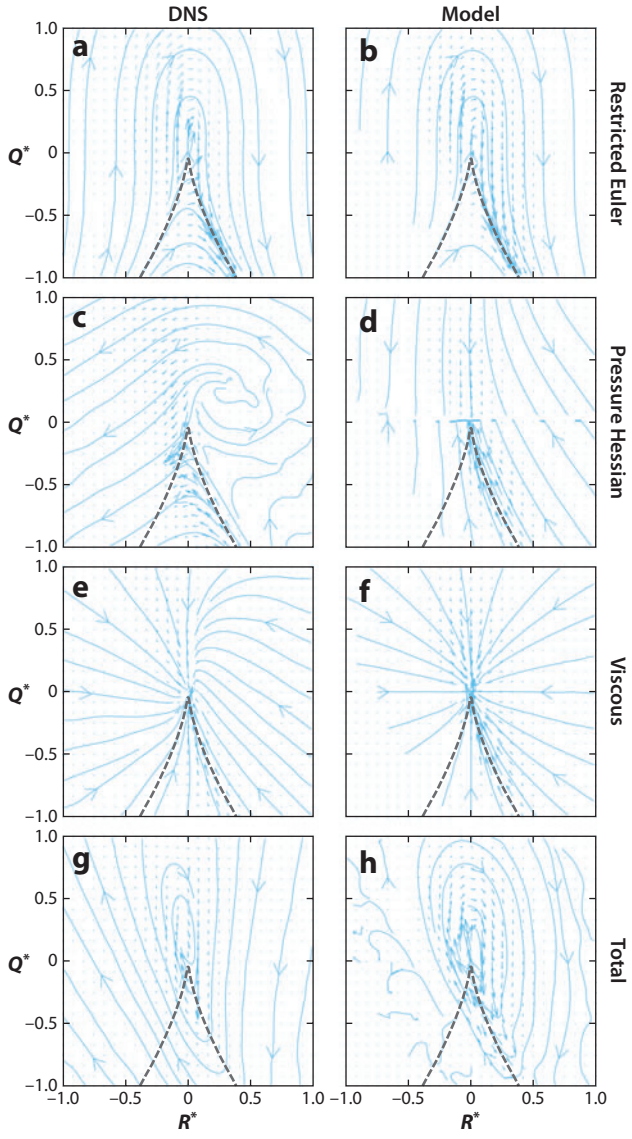


**Figure 8**

Vector and streamline plots of the probability current associated with different terms in the Fokker-Planck equation of velocity gradient evolution, for direct numerical simulation and the recent fluid deformation approximation. (*a*,*b*) Deterministic restricted Euler portion. (*c*,*d*) Flow corresponding to the pressure Hessian. (*e*,*f*) Viscous term. (*g*,*h*) Total current, including the stochastic forcing effects (see Chevillard et al. 2008 for details on how effects from the diffusion and drift terms are evaluated separately). The scale of the vectors is the same in all plots. Figure reproduced from Chevillard et al. (2008).

Annu. Rev. Fluid Mech. 2011.43:219-245. Downloaded from www.annualreviews.org
by JOHNS HOPKINS UNIVERSITY on 03/17/11. For personal use only.

To shed light on the challenge of achieving higher Reynolds numbers, Martins-Afonso & Meneveau (2010) analyzed the time correlations predicted by the model. They found that the temporal autocorrelations of the velocity gradients resulting from the model were significantly longer than the assumed small parameter $\tau_K$ specified in the model. Hence, at decreasing $\tau_K$ (increasing nominal Reynolds number), the assumption underlying the RFDA (decorrelation of **A** after some time $\tau_K$ along the Lagrangian time history) is no longer consistent with the simulated dynamics.

## 3.7. Matrix Shell Model

To remedy the problem of reaching high Reynolds numbers, Biferale et al. (2007) proposed introducing a sequence of velocity gradient tensors for different scales of turbulence. Following

common practice used in so-called shell models (Biferale 2003), the variable is decomposed into contributions from various shells, according to $\mathbf{A} = \sum_n \mathbf{A}^{(n)}$, where each $\mathbf{A}^{(n)}$ describes the velocity gradient in a typical wave-number octave $k_n = 2^n L^{-1}$. Hence, the number of variables grows logarithmically with Reynolds number with eight variables in each shell [as opposed to typically one complex velocity variable used in classical shell models (Biferale 2003)]. The dynamical equation in each shell was proposed as a linear combination of RE dynamics and the classic energy-conserving quadratic shell coupling terms, according to

$$\frac{dA_{ij}^{(n)}}{dt} = \alpha\left(-A_{ik}^{(n)}A_{kj}^{(n)} + \frac{1}{3}A_{mn}^{(n)}A_{nm}^{(n)}\delta_{ij}\right) + (1-\alpha)(F_{ij}^{(n)} - \nu k_n^2 A_{ij}^{(n)}). \quad (39)$$

A wave-number-dependent damping is also added to provide a viscosity- (Reynolds number–) dependent cutoff scale. Following the form of classical shell models (Biferale 2003), the nonlinear term $\mathbf{F}^{(n)}$ depends quadratically on the velocity gradient in neighboring shells ($\mathbf{A}^{n+1}$, $\mathbf{A}^{n-1}$, etc.) in such a way that it conserves the total kinetic energy $\sum_n k_n^{-2}\mathrm{Tr}(\mathbf{A}^{(n)}\mathbf{A}^{(n)^{\mathrm{T}}})$ across all shells. The parameter $\alpha$ determines the relative strength of the local RE self-stretching effects of each shell separately, versus the intershell energy-exchange mechanism. Using numerical integrations of the system with random forcing at the largest scale ($n = 0$ shell), Biferale et al. (2007) showed that such an energy-exchange mechanism was successful at eliminating the RE finite-time divergence. No divergence occurred because all shells ultimately are allowed to exchange kinetic energy with the high-wave-number shells in which viscosity can act strongly. And the presence in each shell of the RE self-stretching mechanism was sufficiently strong to endow the simulated velocity gradient tensors with quite realistic geometric and statistical properties (e.g., the expected vorticity-strain alignment, the shape of $R$, $Q$ joint PDF), at least for the value of $\alpha = 1/2$ tested. Moreover, compared to the single-shell models reviewed above, better results were obtained at high Reynolds numbers (up to 22 shells were tested, corresponding to $R_\lambda = 1{,}500$).

A conceptual drawback of the approach is that the model formulation does not make an explicit connection with the physics of the pressure Hessian. It is not clear how to justify the nonlinear coupling terms based on any physical reasonings about the properties of the pressure Hessian. Another problem is that the increase in the number of degrees of freedom makes it more difficult to develop intuitive understanding of the system.

## 4. OTHER PROPERTIES

The fate of the velocity gradient tensor in turbulence has been recognized as a central issue in various types of turbulent flows. For compressible turbulence, the relevant phase space of invariants also includes $P = \mathrm{Tr}(A)$, and the effects of the pressure Hessian in the equation for $\mathbf{A}$ require different modeling approaches (Lee et al. 2009). This was treated recently by Suman & Girimaji (2009, 2010), who showed that a polytropic equation of state $p = C\rho^n$ can be used to write the pressure Hessian in terms of the Hessian of density. Using the continuity equation $d\rho/dt = -\rho A_{kk}$, taking appropriate derivatives to evaluate the Hessian, and assuming that the spatial gradients of $\mathbf{A}$ are neglected, they derived a closed equation for the pressure Hessian that includes a linear damping term with an inverse relaxation timescale proportional to the divergence, $(n-1)A_{kk}$. The approach shows that in compressible flow, information about past fluid deformation is carried by the density, and this is directly related to the pressure Hessian in this model. The resulting system has been studied in detail by Suman & Girimaji (2010).

When turbulence advects a passive scalar such as a temperature or concentration field $\theta$, the scalar gradient vector $G_i = \partial\theta/\partial x_i$ becomes another interesting property of turbulence small scales worthy of study. Its Lagrangian evolution equation is given by $dG_i/dt = -G_k A_{ki} + \gamma\nabla^2 G_i$.



Annu. Rev. Fluid Mech. 2011.43:219-245. Downloaded from www.annualreviews.org
by JOHNS HOPKINS UNIVERSITY on 03/17/11. For personal use only.

Gonzalez (2009) has applied the RFDA to the diffusion term and studied the time evolution of this system coupled to the system for the velocity gradient tensor. For moderate Reynolds numbers, he found that general features of scalar gradient kinematics such as the production of the scalar gradient norm and alignment with respect to strain principal axes and vorticity are well reproduced. Further generalizations to magnetohydrodynamics, viscoelastic flows, flows with buoyancy, etc., could also be considered.

Another area of considerable practical interest in which the velocity gradients are known to play a crucial role concerns turbulence modeling. For instance, in the context of large-eddy simulation, the subgrid-scale stress tensor $\tau_{ij}$ must be expressed in terms of coarse-grained variables. The coarse-grained velocity gradient tensor $\tilde{\mathbf{A}}$ plays a crucial role in determining the environment in which small-scale fluctuations evolve, giving rise to particular behaviors and alignments of the stress tensor. For instance, in directions perpendicular to strong extension, fluctuations will grow due to vortex stretching. Therefore, it is expected that velocity fluctuations grow in these perpendicular directions. Such effects can be appreciated through the transport equation of the stress tensor that only keeps the production terms

$$\frac{d\boldsymbol{\tau}}{dt} = -\boldsymbol{\tau}\tilde{\mathbf{A}} - \tilde{\mathbf{A}}^T\boldsymbol{\tau}, \tag{40}$$

neglecting pressure-strain correlations, turbulent and viscous diffusion, and viscous damping terms. We refer the reader to Sagaut & Cambon (2008) for a discussion of this pressure-free equation, which we also recognize as equivalent to the equation for the Cauchy-Green tensor treated in prior sections (with opposite signs in the right-hand side). Recognizing (Li et al. 2009) that the analytical solution for constant $\tilde{\mathbf{A}}$ can again be written as $\boldsymbol{\tau}(t) = \exp(-\tilde{\mathbf{A}}t)\cdot\boldsymbol{\tau}(0)\cdot\exp(-\tilde{\mathbf{A}}^T t)$ and applying the RFDA closure to this equation (assuming that the relevant initial condition occurred at some time $\tau$ prior to the present time and that there the upstream initial condition stress tensor is isotropic) lead to a closure for the stress tensor of the form $\boldsymbol{\tau} \sim \exp(-\tilde{\mathbf{A}}\tau)\exp(-\tilde{\mathbf{A}}^T\tau)$. Short-time expansions of the matrix exponentials then lead naturally to eddy-viscosity closures for the deviatoric part of $\boldsymbol{\tau}$, as illustrated by Li et al. (2009). Hence, the nature of Lagrangian time correlations of $\tilde{\mathbf{A}}$ and the associated characteristic decorrelation times as a function of coarse-graining length scale (or filter size) are important components in turbulence modeling.

In recent years, it has been proposed to use visualizations of ridges in the distribution of most positive eigenvalues of the Cauchy-Green tensor or finite-time Lyapunov exponents (also called Lagrangian coherent structures) to understand mixing in various flows and applications (see, e.g., Haller 2002, Voth et al. 2002, Green et al. 2007). Because the Cauchy-Green tensor and the Lagrangian evolution of $\mathbf{A}$ are intimately linked, it is expected that better understanding and models of $\mathbf{A}$ will lead to better predictions of mixing and properties of Lagrangian coherent structures.

Our understanding of velocity gradient dynamics also plays a role in the development and characterization of synthetic turbulence models. Motivated by the RE dynamics, Rosales & Meneveau (2006, 2008) have proposed a multiscale Lagrangian map approach in which a 3D velocity vector field generated by the superposition of random-phase Fourier modes with a prescribed spectrum is deformed as follows: Fluid particles at each position in the volume are displaced with their initial random velocity for a certain time. The velocities are interpolated back to a uniform grid, but the deformation has already concentrated large negative relative velocity and gradients into small portions of the space. This leads to negative skewness, even after the field is projected onto a divergence-free vector field. The basic step is repeated for various length scales in the flow, reproducing a full prescribed energy spectrum. **Figure 9** displays the square velocity gradient that results from such an approach. Detailed statistical analysis (Rosales & Meneveau 2008) shows that

Annu. Rev. Fluid Mech. 2011.43:219-245. Downloaded from www.annualreviews.org
by JOHNS HOPKINS UNIVERSITY on 03/17/11. For personal use only.

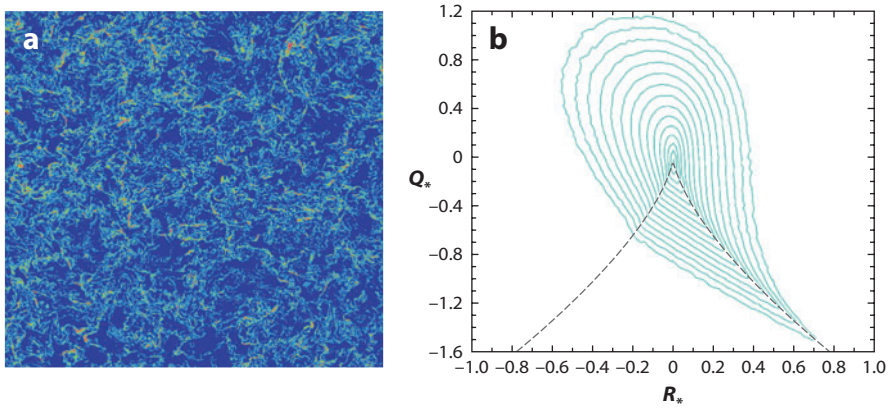


**Figure 9**

(*a*) Contours of square velocity gradients on a planar cut through a 3D synthetic field generated using the multiscale Lagrangian map approach of Rosales & Meneveau (2008). The map concentrates gradients onto small sheet-like structures at which the dissipation occurs and the negative strain skewness originates. (*b*) Joint probability density function of $R$ and $Q$ for synthetic turbulence. Figure adapted from Rosales & Meneveau (2006).

the resulting 3D vector fields display surprisingly realistic statistics such as vorticity alignment, $R$, $Q$ joint PDF, and even anomalous scaling of velocity increment and multifractal structure of the dissipation field. Chevillard et al. (2010) have recently applied the RFDA to the vorticity equation to construct synthetic velocity fields using the Biot-Savart formula.

## 5. CONCLUDING REMARKS

Above we summarize several interesting fundamental properties of small-scale motions in turbulence that can be described using the velocity gradient tensor. We review various models that aim at understanding these phenomena using a small number of ODEs, i.e., a low-dimensional dynamical system or a set of stochastic differential equations. These begin from the gradient of the Navier-Stokes equations and describe the Lagrangian evolution of the velocity gradient tensor elements following fluid particles. They require models for the pressure Hessian and viscous effects. We also review the predictions of the RE system and summarize various models for the pressure Hessian and viscous term. Some generalizations are summarized. Open challenges to achieve arbitrarily high Reynolds numbers with a system for the unfiltered velocity gradient tensor are highlighted.

### SUMMARY POINTS

1. The velocity gradient tensor describes a number of interesting geometrical and statistical phenomena of the fine-scale structure of turbulence, such as the alignment of vorticity with respect to the strain-rate eigenvectors, rate of deformation and shapes of fluid material volumes, non-Gaussian statistics, and intermittency. The coarse-grained or filtered velocity gradient tensor represents such phenomena also at larger scales, for instance, across the inertial range of turbulence.

Annu. Rev. Fluid Mech. 2011.43:219-245. Downloaded from www.annualreviews.org
by JOHNS HOPKINS UNIVERSITY on 03/17/11. For personal use only.

2. Taking the gradient of the Navier-Stokes equations leads to a set of Lagrangian evolution equations describing self-stretching and tilting of the velocity gradient tensor by itself, and additional nonlocal terms due to the pressure Hessian and viscous diffusion.
3. If the nonlocal terms are neglected (RE), analytical solutions for the short-term evolution of the velocity gradient tensor or for some scalar invariants can be obtained that explain several observed trends such as the alignment of vorticity with the strain-rate eigenvectors and the prevalence of axisymmetric expanding motions along the Vieillefosse line $Q = -3/2^{2/3}R^{2/3}$.
4. Models are required for the pressure Hessian and viscous terms. Several models are reviewed here, together with their physical interpretation and predictions. At moderate Reynolds numbers (e.g., $R_\lambda = 150$), the predictions are good. At higher Reynolds numbers, the models written for the unfiltered velocity gradient (i.e., a single shell) show unphysical behavior.

Annu. Rev. Fluid Mech. 2011.43:219-245. Downloaded from www.annualreviews.org
by JOHNS HOPKINS UNIVERSITY on 03/17/11. For personal use only.

### FUTURE ISSUES

1. The Lagrangian evolution equation for **A**, consisting of a small number of coupled nonlinear ODEs (eight in incompressible flow), provides a drastic reduction of complexity compared with the infinite-dimensional Navier-Stokes equation. It promises that still much further progress can be made in our fundamental understanding of universal properties of the turbulence small-scale structure by working on improved Lagrangian models for **A**.
2. Significant challenges remain to develop models for the pressure Hessian and the viscous term that may be applied to arbitrarily high Reynolds numbers. Developing such models would be useful to better understand Reynolds number scaling, intermittency, and the asymptotic structure of turbulence.
3. For the coarse-grained velocity gradient, understanding of the trends as a function of scale requires more in-depth understanding of the gradient of the subgrid-scale stress tensor and its conditional statistics. Progress along these lines may prove fruitful in formulating and understanding improved subgrid-scale models of turbulence.
4. Generalizations of the Lagrangian models and the various closure methods summarized here to other gradient fields (e.g., gradients of magnetic field, active scalars, and viscoelastic flow) may prove to be a fruitful area of research.

## DISCLOSURE STATEMENT

The author is not aware of any funding or financial holdings that might be perceived as affecting the objectivity of this review.

## ACKNOWLEDGMENTS

The insights that shape the author's views have arisen from collaborations with Yi Li, Laurent Chevillard, Carlos Rosales, Marco Martins-Afonso, and Huidan Yu. Their contributions

are gratefully acknowledged. Financial support has been provided by NSF-ITR, NSF-CBET, and the Keck Foundation. The author is grateful to Gregory Eyink, Alex Szalay, Ethan Vishniac, and Shiyi Chen for many discussions; to Huidan Yu for help with **Figure 1*c*** and for useful comments; and to Stephen B. Pope, Alain Pumir, Laurent Chevillard, and Yi Li for comments on a draft version of this manuscript.

## LITERATURE CITED

Anselmet F, Gagne Y, Hopfinger EJ, Antonia RA. 1984. High-order velocity structure functions in turbulent shear flows. *J. Fluid Mech.* 140:63–89

Ashurst WT, Kerstein AR, Kerr RM, Gibson CH. 1987. Alignment of vorticity and scalar gradient with the strain rate in simulated Navier-Stokes turbulence. *Phys. Fluids* 30:2343–53

Batchelor GK. 1952. The effect of homogeneous turbulence on material lines and surfaces. *Proc. R. Soc. Lond. A* 213:349–66

Biferale L. 2003. Shell models of energy cascade in turbulence. *Annu. Rev. Fluid Mech.* 35:441–68

Biferale L, Chevillard L, Meneveau C, Toschi F. 2007. Multiscale model of gradient evolution in turbulent flows. *Phys. Rev. Lett.* 98:214501

Bikkani RK, Girimaji SS. 2007. Role of pressure in nonlinear velocity gradient dynamics in turbulence. *Phys. Rev. E* 75:036307

Borue V, Orszag SA. 1998. Local energy flux and subgrid-scale statistics in three-dimensional turbulence. *J. Fluid Mech.* 366:1–31

Brasseur JG, Lin W. 2002. Kinematics and dynamics of small-scale vorticity and strain-rate structures in the transition from isotropic to shear turbulence. *Fluid Dyn. Res.* 36:357–84

Cantwell BJ. 1992. Exact solution of a restricted Euler equation for the velocity gradient tensor. *Phys. Fluids A* 4:782–93

Cantwell BJ. 1993. On the behavior of velocity gradient tensor invariants in direct numerical simulations of turbulence. *Phys. Fluids A* 5:2008–13

Cantwell BJ. 2002. A singularity-free model of the local velocity gradient and acceleration gradient structure of turbulent flow. In *Tubes, Sheets and Singularities in Fluid Dynamics, Proc. IUTAM Symp. Zakopane, Poland*, ed. K Bajer, HK Moffatt, pp. 247–60. New York: Springer

Castaing B, Gagne Y, Hopfinger EJ. 1990. Velocity probability density functions of high Reynolds number turbulence. *Physica D* 46:177–200

Chertkov M, Pumir A, Shraiman BI. 1999. Lagrangian tetrad dynamics and the phenomenology of turbulence. *Phys. Fluids* 11:2394–410

Chevillard L, Castaing B, Lévêque E, Arneodo A. 2006. Unified multifractal description of velocity increments statistics in turbulence: intermittency and skewness. *Physica D* 218:77–82

Chevillard L, Meneveau C. 2006. Lagrangian dynamics and statistical geometric structure of turbulence. *Phys. Rev. Lett.* 97:174501

Chevillard L, Meneveau C. 2007. Intermittency and universality in a Lagrangian model of velocity gradients in three-dimensional turbulence. *C.R. Méc.* 335:187–93

Chevillard L, Meneveau C, Biferale L, Toschi F. 2008. Modeling the pressure Hessian and viscous Laplacian in turbulence: comparisons with direct numerical simulation and implications on velocity gradient dynamics. *Phys. Fluids* 20:101504

Chevillard L, Robert R, Vargas V. 2010. A stochastic representation of the local structure of turbulence. *Eur. Phys. Lett.* 89:54002

Chong MS, Perry AE, Cantwell BJ. 1990. A general classification of three-dimensional flow fields. *Phys. Fluids A* 2:765–77

Chong MS, Soria J, Perry AE, Chacin J, Cantwell BJ, Na Y. 1998. Turbulence structures of wall-bounded shear flows found using DNS data. *J. Fluid Mech.* 357:225–47

Cocke WJ. 1969. Turbulent hydrodynamic line stretching: consequences of isotropy. *Phys. Fluids* 12:2448–92

Elsinga GE, Marusic I. 2010. Evolution and lifetimes of flow topology in a turbulent boundary layer. *Phys. Fluids* 22:015102

Annu. Rev. Fluid Mech. 2011.43:219-245. Downloaded from www.annualreviews.org
by JOHNS HOPKINS UNIVERSITY on 03/17/11. For personal use only.

Festa R, Mazzino A, Tizzi M. 2007. Route to non-Gaussian statistics in convective turbulence. *Phys. Rev. E* 75:035301

Frisch U. 1995. *Turbulence: The Legacy of A.N. Kolmogorov*. Cambridge, UK: Cambridge Univ. Press

Galanti B, Gibbon JD, Heritage M. 1997. Vorticity alignment results for the three-dimensional Euler and Navier-Stokes equations. *Nonlinearity* 10:1675–94

Gibbon JD, Holm DD. 2007. Lagrangian particle paths and ortho-normal quaternion frames. *Nonlinearity* 20:1745–59

Girimaji SS, Pope SB. 1990a. A diffusion model for velocity gradients in turbulence. *Phys. Fluids A* 2:242–56

Girimaji SS, Pope SB. 1990b. Material element deformation in isotropic turbulence. *J. Fluid Mech.* 220:427–58

Girimaji SS, Speziale CG. 1995. A modified restricted Euler equation for turbulent flows with mean velocity gradients. *Phys. Fluids* 7:1438–46

Gonzalez M. 2009. Kinematic properties of passive scalar gradient predicted by a stochastic Lagrangian model. *Phys. Fluids* 21:055104

Goto T, Kida S. 2002. A multiplicative process of material line stretching by turbulence. *J. Turbul.* 3:17

Green M, Rowley CW, Haller G. 2007. Detection of Lagrangian coherent structures in three-dimensional turbulence. *J. Fluid Mech.* 572:111–20

Guala M, Lüthi B, Liberzon A, Tsinober A, Kinzelbach W. 2005. On the evolution of material lines and vorticity in homogeneous turbulence. *J. Fluid Mech.* 533:339–59

Gulitski G, Kholmyansky M, Kinzelbach W, Lüthi B, Tsinober A, Yorish Y. 2007. Velocity and temperature derivatives in high-Reynolds-number turbulent flows in the atmospheric surface layer. Part 1. Facilities, methods and some general results. *J. Fluid Mech.* 589:57–81

Haller G. 2002. Lagrangian coherent structures from approximate velocity data. *Phys. Fluids* 14:1851–61

Higgins CW, Parlange MB, Meneveau C. 2003. Alignment trends of velocity gradients and subgrid-scale fluxes in the turbulent atmospheric boundary layer. *Bound. Layer Meteorol.* 109:59–83

Ishihara T, Gotoh T, Kaneda Y. 2009. Study of high Reynolds number isotropic turbulence by direct numerical simulation. *Annu. Rev. Fluid Mech.* 41:165–80

Jeong E, Girimaji SS. 2003. Velocity-gradient dynamics in turbulence: effect of viscosity and forcing. *Theoret. Comput. Fluid Dyn.* 16:421–32

Jimenez J. 1992. Kinematic alignment effects in turbulent flows. *Phys. Fluids A* 4:652–54

Kailasnath P, Sreenivasan KR, Stolovitzky G. 1992. Probability density of velocity increments in turbulent flows. *Phys. Rev. Lett.* 68:2766–69

Katz J, Sheng J. 2010. Applications of holography in fluid mechanics and particle dynamics. *Annu. Rev. Fluid Mech.* 42:531–55

Kerr RM. 1987. Histograms of helicity and strain in numerical turbulence. *Phys. Rev. Lett.* 59:783–86

Lee K, Girimaji SS, Kerimo J. 2009. Effect of compressibility on turbulent velocity gradients and small scale structure. *J. Turbul.* 10:9

Léorat J. 1975. *La turbulence magnétohydrodynamique hélicitaire et génération des champs magnétique a grande échelle*. PhD thesis. Univ. Paris VII

Li Y, Chevillard L, Meneveau C, Eyink G. 2009. Matrix exponential-based closures for the turbulent subgrid-scale stress tensor. *Phys. Rev. E* 79:016305

Li Y, Meneveau C. 2005. On the origin of non-Gaussian statistics in hydrodynamic turbulence. *Phys. Rev. Lett.* 95:164502

Li Y, Meneveau C. 2006. Intermittency trends and Lagrangian evolution of non-Gaussian statistics in turbulent flow and scalar transport. *J. Fluid Mech.* 558:133–42

Li Y, Meneveau C. 2007. Material deformation in a restricted Euler model for turbulent flows: analytic solution and numerical tests. *Phys. Fluids* 19:015104

Li Y, Perlman E, Wan M, Yang Y, Meneveau C, et al. 2008. A public turbulence database cluster and applications to study Lagrangian evolution of velocity increments in turbulence. *J. Turbul.* 9:31

Lund TS, Rogers MM. 1994. An improved measure of strain state probability in turbulent flows. *Phys. Fluids* 6:1838–47

Lüthi B, Holzner M, Tsinober A. 2009. Expanding the QR space to three dimensions. *J. Fluid Mech.* 641:497–507

Annu. Rev. Fluid Mech. 2011.43:219-245. Downloaded from www.annualreviews.org
by JOHNS HOPKINS UNIVERSITY on 03/17/11. For personal use only.

Lüthi B, Tsinober A, Kinzelbach W. 2005. Lagrangian measurement of vorticity dynamics in turbulent flow. *J. Fluid Mech.* 528:87–118
Martin J, Dopazo C, Valiño L. 1998a. Dynamics of velocity gradient invariants in turbulence: restricted Euler and linear diffusion models. *Phys. Fluids* 10:2012–25
Martin J, Ooi A, Chong MS, Soria J. 1998b. Dynamics of the velocity gradient tensor invariants in isotropic turbulence. *Phys. Fluids* 10:2336–46
Martins-Afonso M, Meneveau C. 2010. Recent fluid deformation closure for velocity gradient tensor dynamics in turbulence: timescale effects and expansions. *Physica D* 239:1241–50
Meneveau C, Sreenivasan KR. 1991. The multifractal nature of turbulent energy dissipation. *J. Fluid Mech.* 224:429–84
Mullin JA, Dahm WJA. 2006. Dual-plane stereo particle image velocimetry measurements of velocity gradient tensor fields in turbulent shear flow. II. Experimental results. *Phys. Fluids* 18:035102
Naso A, Pumir A. 2005. Scale dependence of the coarse-grained velocity derivative tensor structure in turbulence. *Phys. Rev. E* 72:056318
Naso A, Pumir A, Chertkov M. 2006. Scale dependence of the coarse-grained velocity derivative tensor: influence of large-scale shear on small-scale turbulence. *J. Turbul.* 7:41
Naso A, Chertkov M, Pumir A. 2007. Statistical geometry in homogeneous and isotropic turbulence. *J. Turbul.* 8:39
Nelkin M. 1990. Multifractal scaling of velocity derivatives in turbulence. *Phys. Rev. A* 42:7226–29
Nomura KK, Post GK. 1998. The structure and dynamics of vorticity and rate of strain in incompressible homogeneous turbulence. *J. Fluid Mech.* 377:65–97
Ooi A, Martin J, Soria J, Chong MS. 1999. A study of the evolution and characteristics of the invariants of the velocity-gradient tensor in isotropic turbulence. *J. Fluid Mech.* 381:141–74
Perry AE, Chong MS. 1987. A description of eddying motions and flow patterns using critical-point concepts. *Annu. Rev. Fluid Mech.* 19:125–55
Pope SB, Chen YL. 1990. The velocity-dissipation probability density function model for turbulent flows. *Phys. Fluids A* 2:1437–49
Pumir A, Shraiman BI. 2003. Lagrangian particle approach to large eddy simulations of hydrodynamic turbulence. *J. Stat. Phys.* 113:693–700
Pumir A, Shraiman BI, Chertkov M. 2000. Geometry of Lagrangian dispersion in turbulence. *Phys. Rev. Lett.* 85:5324–27
Rosales C, Meneveau C. 2006. A minimal multiscale Lagrangian map approach to synthesize non-Gaussian turbulent vector fields. *Phys. Fluids* 18:075104
Rosales C, Meneveau C. 2008. Anomalous scaling and intermittency in three-dimensional synthetic turbulence. *Phys. Rev. E* 78:016313
Sagaut P, Cambon C. 2008. *Homogeneous Turbulence Dynamics*. Cambridge, UK: Cambridge Univ. Press
She ZS, Jackson E, Orszag SA. 1991. Structure and dynamics of homogeneous turbulence: models and simulations. *Proc. R. Soc. Math. Phys. Sci.* 434:101–24
Soria J, Sondergaard R, Cantwell BJ, Chong MS, Perry AE. 1998. A study of the fine-scale motions of incompressible time-developing mixing layers. *Phys. Fluids* 6:871–84
Sreenivasan KR, Antonia RA. 1997. The phenomenology of small-scale turbulence. *Annu. Rev. Fluid Mech.* 29:435–72
Suman S, Girimaji SS. 2009. Homogenized Euler equation: a model for compressible velocity gradient dynamics. *J. Fluid Mech.* 620:177–94
Suman S, Girimaji SS. 2010. Velocity gradient invariants and local flow-field topology in compressible turbulence. *J. Turbul.* 11:2
Tao B, Katz J, Meneveau C. 2002. Statistical geometry of subgrid-scale stresses determined from holographic particle image velocimetry measurements. *J. Fluid Mech.* 457:35–78
Tsinober A. 2009. *An Informal Conceptual Introduction to Turbulence*. New York: Springer. 2nd ed.
Tsinober A, Kit E, Dracos T. 1992. Experimental investigation of the field of velocity gradients in turbulent flows. *J. Fluid Mech.* 242:169–92
Van der Bos F, Tao B, Meneveau C, Katz J. 2002. Effects of small-scale turbulent motions on the filtered velocity gradient tensor as deduced from holographic PIV measurements. *Phys. Fluids* 14:2456–74

Annu. Rev. Fluid Mech. 2011.43:219-245. Downloaded from www.annualreviews.org
by JOHNS HOPKINS UNIVERSITY on 03/17/11. For personal use only.

Vieillefosse P. 1982. Local interaction between vorticity and shear in a perfect incompressible fluid. *J. Phys.* (*Paris*) 43:837–42

Vieillefosse P. 1984. Internal motion of a small element of fluid in an inviscid flow. *Phys. A* 125:150–62

Voth GA, Haller G, Gollub JP. 2002. Experimental measurements of stretching fields in fluid mixing. *Phys. Rev. Lett.* 88:254501

Wallace JM. 2009. Twenty years of experimental and direct numerical simulation access to the velocity gradient tensor: What have we learned about turbulence? *Phys. Fluids* 21:021301

Wallace JM, Vukoslavcevic PV. 2010. Measurement of the velocity gradient tensor in turbulent flows. *Annu. Rev. Fluid Mech.* 42:157–81

Yeung PK, Pope SB. 1989. Lagrangian statistics from direct numerical simulations of isotropic turbulence. *J. Fluid Mech.* 207:531–86

Yeung PK, Pope SB, Lamorgese AG, Donzis DA. 2005. Acceleration and dissipation statistics of numerically simulated isotropic turbulence. *Phys. Fluids* 18:065103

Zeff BW, Lanterman DD, McAllister R, Roy R, Kostelich EJ, Lathrop DP. 2003. Measuring intense rotation and dissipation in turbulent flows. *Nature* 421:146–49

Annu. Rev. Fluid Mech. 2011.43:219-245. Downloaded from www.annualreviews.org
by JOHNS HOPKINS UNIVERSITY on 03/17/11. For personal use only.

Annual Review of
Fluid Mechanics

Volume 43, 2011

# Contents



Annu. Rev. Fluid Mech. 2011.43:219-245. Downloaded from www.annualreviews.org
by JOHNS HOPKINS UNIVERSITY on 03/17/11. For personal use only.

**Indexes**



**Errata**

An online log of corrections to *Annual Review of Fluid Mechanics* articles may be found at http://fluid.annualreviews.org/errata.shtml



Annu. Rev. Fluid Mech. 2011.43:219-245. Downloaded from www.annualreviews.org
by JOHNS HOPKINS UNIVERSITY on 03/17/11. For personal use only.